



ELSEVIER

Control Engineering Practice ■ (■■■■) ■■■-■■■

CONTROL ENGINEERING
PRACTICEwww.elsevier.com/locate/conengprac

Robust vehicle yaw control using an active differential and IMC techniques

M. Canale^{a,*}, L. Fagiano^a, M. Milanese^a, P. Borodani^b

^a*Dipartimento di Automatica e Informatica, Politecnico di Torino, Corso Duca degli Abruzzi, 24-10129 Torino, Italy*

^b*Centro Ricerche Fiat, Vehicles Department, Vehicle Control Systems, Strada Torino, 50-10043 Orbassano (TO), Italy*

Received 7 June 2006; accepted 30 November 2006

Abstract

A robust non-parametric approach to improve vehicle yaw rate dynamics by means of a rear active differential is introduced. An additive model set is used to describe the uncertainty arising from the wide range of the vehicle operating situations. The design of the feedback controller is performed using an enhanced internal model control (IMC) technique, able to handle in an effective way both robustness and control variable saturation issues. In order to improve the transient behaviour a feedforward control contribution has been added giving rise to a two degree of freedom structure. Improvements on understeering characteristics, stability in demanding conditions such as μ -split braking and damping properties in reversal steer and low friction step steer manoeuvres are shown through simulation results performed on an accurate 14 degrees of freedom non-linear model of a segment D car.

© 2006 Elsevier Ltd. All rights reserved.

Keywords: Automotive control; Active control; Yaw rate; Uncertainty; Robust control; Constraints

1. Introduction

Vehicle yaw dynamics may show unexpected dangerous behaviour in presence of unusual external conditions such as lateral wind force, different left-right side friction coefficients and steering steps needed to avoid obstacles. Moreover, in standard cornering manoeuvres understeering phenomena may deteriorate handling performances in manual driving and cause uncomfortable feelings to the human driver. Vehicle active control systems aim to enhance handling and comfort characteristics ensuring stability in critical situations. In this context, several solutions have been proposed in recent years and the topic is still an object of intense research activities from both industrial and academic sides (see e.g. Ackermann & Sienel, 1993; Ackermann, Guldner, Steinhausner, & Utkin, 1995; Assadian & Hancock, 2005; Börner & Isermann, 2006; Colombo, 2005; Gaspar, Szaszi, & Bokor, 2005; Gerhard et al., 2005; Güvenç, Bünte, & Güvenç, 2004;

Kohen & Ecrick, 2004; Malan, Taragna, Borodani, & Gortan, 1994; Mokhiamar & Abe, 2002; van Zanten, 2000 van Zanten, Erhart, & Pfaff, 1995; Vilaplana, Mason, Leith, & Leithead, 2005; Zheng, Tang, Han, & Zhang, 2006). All the proposed strategies modify the vehicle dynamics exploiting appropriate combinations of longitudinal and/or lateral tyre forces. In fact, the yaw moments required to impose a desired car behaviour can be generated by means of unsymmetrical longitudinal force distributions in left-right sides of the vehicle axles. This can be realized through different technologies such as active braking actions employed in ABS, VDC and ESP systems (see e.g. van Zanten, 2000; van Zanten et al., 1995) or left-right driving torque distribution by means of active differential devices (see e.g. Assadian & Hancock, 2005; Colombo, 2005; Gerhard et al., 2005). Besides, the action of superimposed front and/or rear steering angles in four wheel steer by wire vehicles can be exploited to generate the distribution of lateral forces needed to modify the vehicle dynamics (see e.g. Ackermann & Sienel, 1993; Ackermann et al., 1995; Kohen & Ecrick, 2004; Vilaplana et al., 2005). Moreover, an interesting area of research consists in

*Corresponding author. Tel.: +39 011 5647063; fax: +39 011 5647099.

E-mail address: massimo.canale@polito.it (M. Canale).

optimizing the actions of both a direct yaw control and active wheel steering to achieve good safety properties in face of sudden manoeuvres (see e.g. Mokhiemar & Abe, 2002). However, a key point is the fact that not every required combination of tyre forces can be generated, due to physical limitations of actuators and tyres. Thus the input variable, whatever it is, may saturate and this could deteriorate the control performances. In addition, as the vehicle operates under a wide range of conditions of speed, load, friction etc., the active control system has to guarantee safety (i.e. stability) robustly in face of the uncertainty arising from such operating situations. Robustness of active vehicle systems is a widely studied topic and interesting results have appeared in both parametric and non-parametric contexts (see e.g. Ackermann et al., 1995; Gerhard et al., 2005; Guvenc et al., 2004; Malan et al., 1994). As a consequence, the designer of the control system has to take care of both robust stability and control saturation aspects. In this paper, the problem of yaw control is considered for a vehicle equipped with a rear active differential (RAD) device developed and patented at Centro Ricerche Fiat (Frediani, Gianoglio, & Giuliano, 2002; Ippolito, Lupo, & Lorenzini, 1992). As to the choice of the control structure to be adopted, a feedforward-feedback scheme is considered. The feedforward contribution is used to enhance system performances in the transient phase while the feedback controller is designed to guarantee robust stability and to optimize the behaviour when the yaw moment provided by RAD is saturated. Given this requirements, internal model control (IMC) techniques are used in the design of the feedback controller as they are well established control methodologies able to handle in an effective way both robustness (see Morari & Zafiriou, 1989) and saturation (see e.g. Goodwin, Graebe, & Levine, 1993; Zheng, Kothare, & Morari, 1994) issues. In particular, the enhanced IMC structure presented in Canale (2004), which guarantees robust stability as well as improved performances during saturation, will be employed. As such design methodology is based on robust H_∞ optimization techniques, a linear model of the lateral vehicle dynamics will be considered and an unstructured uncertainty description approach will be adopted to take into account the different operating conditions of the vehicle. The effectiveness of the proposed control approach is shown by means of simulation results obtained using a detailed nonlinear 14 degrees of freedom vehicle model of a segment D Alfa Romeo prototype which proved to give an accurate description of the vehicle dynamics as compared to actual measurements (see Colombo, 2005). The paper is organized as follows: in Section 2 the problem definition and the control requirements are introduced; in Section 3 the vehicle modelling aspects are discussed. In Section 4 the proposed control structure is introduced and its design principles are described. Finally, in Section 5, quite extensive simulation results are presented in order to show the effectiveness of the presented control strategy.

2. Problem formulation and control requirements

Vehicle yaw control aim is to change steady state and transient properties of the car, enhancing vehicle handling in cornering manoeuvres and keeping stability in presence of unusual external conditions and inputs, such as lateral wind force or different left–right side friction coefficients. In order to introduce the control system objectives, it is useful to briefly recall basic concepts on vehicle cornering behaviour. The vehicle inputs are steering angle, commanded by the driver, and external forces and moments applied to the vehicle e.g. by an active device. The most significant variables describing vehicle behaviour are lateral acceleration $a_y(t)$, yaw rate $\dot{\psi}(t)$ and vehicle sideslip angle $\beta(t)$. As a first approximation, considering car and suspension system as a rigid body moving at constant speed v , the following relationship links $a_y(t)$ to $\dot{\psi}(t)$ and $\dot{\beta}(t)$:

$$a_y(t) = v(\dot{\psi}(t) + \dot{\beta}(t)). \quad (1)$$

In steady state motion vehicle sideslip angle is constant and lateral acceleration is therefore proportional to yaw rate through the vehicle speed.

In this situation, let us consider an uncontrolled car. For each constant speed value, by means of standard steering pad manoeuvres it is possible to obtain the steady state lateral acceleration corresponding to different values of the steering angle. These values can be graphically represented on the vehicle *understeering* curve (see Fig. 1, dotted line) where the steering angle δ is reported with respect to the lateral acceleration. Such curves are mostly influenced by road friction and depend on the tyre lateral force-slip characteristics. The curve course may be divided into two zones: at low acceleration the shape is linear and its slope is a measure of the readiness of the car: the lower this value, the higher the lateral acceleration reached by the vehicle with the same steering wheel angle, the more the sport feeling and handling quality perceived by the driver (see e.g. Data & Frigerio, 2002); at high acceleration values the

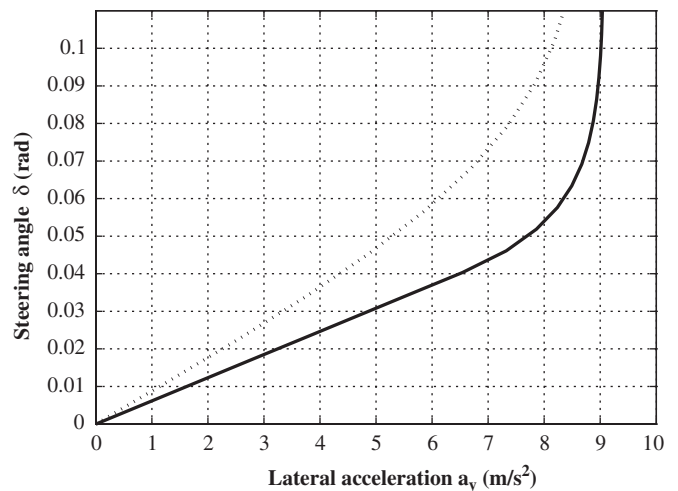


Fig. 1. Uncontrolled vehicle (dotted), and target (solid) understeering curves. Vehicle speed: 100 km/h.

course becomes non-linear showing a saturation value, that is the highest lateral acceleration the vehicle can reach. An external force or moment acting on the car centre of gravity is able to vary, under the same steering conditions, the behaviour of a_y , improving the vehicle maximum lateral acceleration and modifying the understeering curve slope according to some desired requirements. The enhancements obtained by the intervention of an additional yaw moment can be described by means of an improved understeering curve (as shown in Fig. 1, solid line), which can be considered as a target performance to be obtained by the control system. More details about the generation of such target understeering curves will be reported in Section 4.1.

In this context, the choice of yaw rate as the controlled variable is justified as a control action on $\dot{\psi}$ directly influences the behaviour of a_y . Moreover $\dot{\psi}$ can be easily measured by quite standard on board instrumentation. A reference generator will provide the values for $\dot{\psi}$ needed to achieve the desired performances by means of a suitably designed feedback control law.

As to the yaw moment generation, in this paper a full active rear differential developed and patented at Centro Ricerche FIAT (Frediani et al., 2002; Ippolito et al., 1992) is used. In particular, the device considered in this work has a yaw moment limitation of 2500 Nm. The main advantage of this system is the capability of generating yaw moment of every value within the actuation system saturation limits, regardless of the input driving torque value and the speed values of the rear wheels. The control system working area is therefore larger than that of other controlled differential solutions and it is limited only by the actuation system mechanical limits, as shown by the results obtained by Centro Ricerche FIAT, which developed several control strategies for this device and tested them on physical prototypes, with different road friction conditions (see Avenati, Campo, & Ippolito, 1998; Colombo, 2005).

As previously described, the improvements on the understeering performances may be obtained using suitable modifications of the vehicle yaw dynamics in steady state conditions. As a matter of fact also in critical manoeuvring situations such as fast path changing at high speed or braking and steering with low and non-uniform road friction the vehicle dynamics need to be improved in order to enhance stability and handling performances. In particular, given the swiftness of such manoeuvres the transient vehicle behaviour needs to satisfy good damping and readiness properties. This can be taken into account by the feedback design imposing well damped closed loop characteristics and by means of a feedforward action based on the driver input (i.e. δ) to increase system readiness. Needless to say that at least safety (i.e. stability) requirements have to be guaranteed in face of the uncertainty arising from the wide range of the vehicle operating conditions of speed, load, tyre, friction etc. This can be achieved by performing a robust controller design using an appropriate description of the uncertainty as it will be

described in the following Sections 3 and 4. Moreover, in order to take into account the effects of yaw moment saturation, the controller structure should be provided by suitable implementation solutions like anti-windup schemes to improve the system performances in such situation.

3. Model structure description

3.1. Vehicle dynamics modelling

Control design will be worked out on the basis of the single track vehicle model reported in Fig. 2, with tyre dynamic force generation description. The employed model is based on the following hypothesis:

- Flat road.
- Longitudinal motion resistances are ignored compared to wheel lateral forces.
- No rear wheel steering angle.
- Wheel self aligning moments are ignored.
- Steering angle and vehicle sideslip angle are small enough to linearize their trigonometrical functions.
- Vehicle speed is a known parameter, vehicle longitudinal acceleration is low or equal to zero.

Tyre lateral force-sideslip linear dependence is obtained by linearizing Pacejka formulation (see Bakker, Lidner, & Pacejka, 1989), with slip angle in the neighbourhood of the origin. The dynamic generation mechanism of tyre forces is also modelled by introducing tyre lateral relaxation lengths.

Thus, for the considered model, dynamic equations are the following:

$$\begin{aligned} mv(t)\dot{\beta}(t) + mv(t)\dot{\psi}(t) &= F_{yf,p}(t) + F_{yr,p}(t), \\ J_z\ddot{\psi}(t) &= aF_{yf,p}(t) - bF_{yr,p}(t) + M_z(t), \\ F_{yf,p}(t) + \dot{F}_{yf,p}(t)l_f/v(t) &= -c_f(\beta(t) + a\dot{\psi}(t)/v(t) - \delta(t)), \\ F_{yr,p}(t) + \dot{F}_{yr,p}(t)l_r/v(t) &= -c_r(\beta(t) - b\dot{\psi}(t)/v(t)), \end{aligned} \quad (2)$$

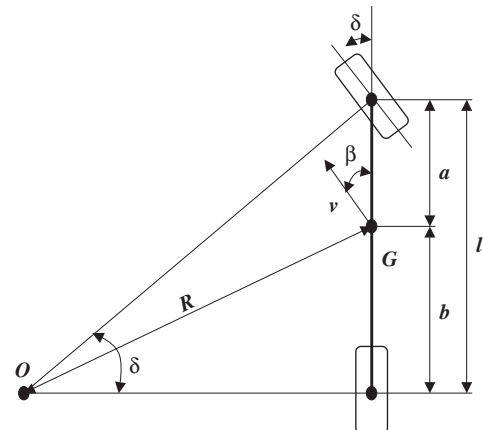


Fig. 2. Single track schematic.

where m is the vehicle mass, J_z is the moment of inertia around the vertical axis, l is the wheel base, a and b are the distances between the centre of gravity and the front and rear axles, respectively, l_f and l_r are the front and rear tyre relaxation lengths, c_f and c_r are the front and rear tyre cornering stiffnesses. $F_{yf,p}$ and $F_{yr,p}$ are the front and rear tyre lateral forces, δ is the front steering angle, β is the vehicle sideslip angle, ψ is the vehicle yaw angle and v is the vehicle speed.

Using Eqs. (2), the vehicle yaw rate dynamics can be described for a fixed vehicle speed value v , by the following transfer functions in the Laplace domain:

$$\dot{\psi}(s) = G_\delta(s)\delta(s) + G_M(s)M_z(s), \quad (3)$$

where

$$G_\delta(s) = \frac{b_2s^2 + b_1s + b_0}{a_4s^4 + a_3s^3 + a_2s^2 + a_1s + a_0},$$

$$G_M(s) = \frac{c_3s^3 + c_2s^2 + c_1s + c_0}{a_4s^4 + a_3s^3 + a_2s^2 + a_1s + a_0} \quad (4)$$

and

$$a_4 = mJ_zl_fl_r, \quad a_3 = mvJ_z(l_f + l_r),$$

$$a_2 = J_z(mv^2 + c_fl_r + c_rl_f) + m(c_fa^2l_r + c_rb^2l_f),$$

$$a_1 = v(J_z(c_f + c_r) + m(c_fa(a - l_r) + c_rb(b + l_f))),$$

$$a_0 = c_fc_rl^2 - mv^2(c_fa - c_rb),$$

$$b_2 = mvac_rl_r, \quad b_1 = mv^2ac_f, \quad b_0 = vvc_rl,$$

$$c_3 = ml_fl_r, \quad c_2 = mv(l_f + l_r)$$

$$c_1 = mv^2 + c_fl_r + c_rl_f, \quad c_0 = v(c_f + c_r). \quad (5)$$

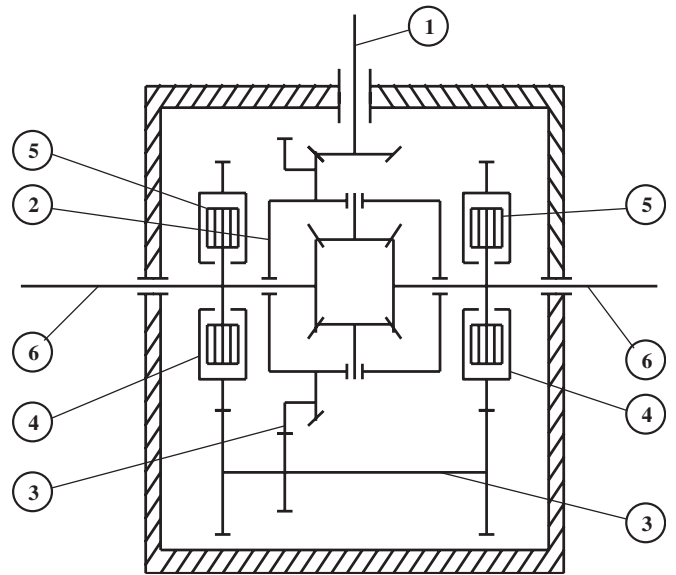


Fig. 3. Rear active differential schematic. The input shaft 1 transfers driving power to the traditional bevel gear differential 2 and, through the additional gearing 3, to the clutch housings 4. Clutch discs 5 are fixed to the output axles 6.

3.2. Actuation system modelling

A schematic of the RAD taken into account in this paper is reported in Fig. 3. The device is basically a traditional bevel gear differential that has been modified in order to transfer motion to two clutch housings, which rotate together with the input gear. Clutch friction discs are fixed on each differential output axle. The ratio between the input angular speed of the bevel gear differential and the angular speeds of the clutch housings is such that the latter rotate faster than their respective discs in almost every vehicle motion condition (i.e. except for narrow cornering at very low vehicle speed), thus the sign of each clutch torque is always known and the torque magnitude only depends on the clutch actuation force, which is generated by an electro-hydraulic system whose input current I_M is determined by the controller. For example, the generation of an actuation force on the left clutch has the effect of transmitting driving torque from the right wheel to the left one: the difference between longitudinal right and left driving forces generates the yaw moment requested by the control system. The dynamic characteristics of this device are dominated by the properties of the hydraulic valves which regulate the fluid pressure needed to generate the clutch closing forces by means of hydraulic pistons. In Fig. 4 the results of a typical step test performed on the electro-hydraulic valve are shown.

It is evident from Fig. 4 that the actuator dynamics can be described by a first order model as

$$G_A(s) = \frac{M_z(s)}{I_M(s)} = G'_A(s) e^{-\theta_A s},$$

$$G'_A(s) = \bar{K}_A \frac{K_A}{1 + s/\omega_A}, \quad (6)$$

where I_M is the input current originated by the controller and M_z is the actual yaw moment provided by RAD to the

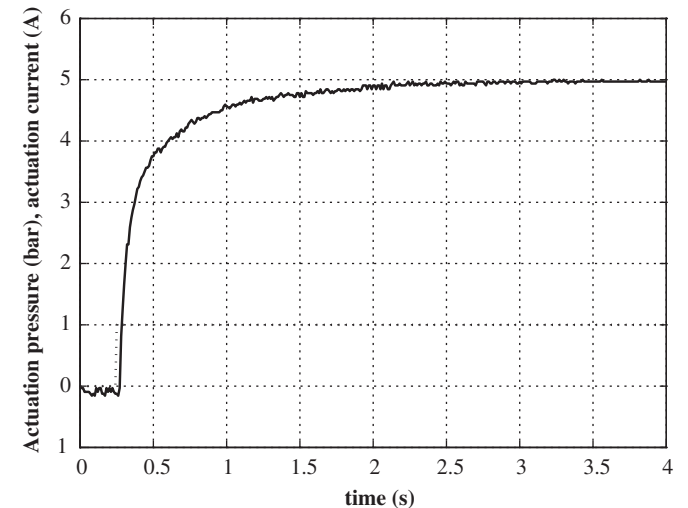


Fig. 4. Example of an actuation system test: valve current step input of 1 A at 100 A/s (dotted) and measured pressure output (solid).

vehicle. The gain \bar{K}_A is defined as

$$\bar{K}_A = \frac{S_A \mu_A \bar{r}_A t_V}{r_W},$$

where S_A is the effective hydraulic piston area, μ_A is the clutch friction coefficient, \bar{r}_A is the clutch mean radius, t_V is the distance from the left to the right ideal rear force application points between the wheels and the ground and r_W is the effective radius of the rear wheels. The electro-hydraulic valve behaviour is defined by means of the bandwidth ω_A , the delay ϑ_A and the gain K_A . As a matter of fact, pure time delays may occur in the conversion of the valve pressure into the required yaw moment. Such delays depend on the entity of the generated torque and are difficult to characterize. Anyway rough estimates of such delays have shown that their entity is of the order of few milliseconds. Indeed, their effects can be taken into account by including them in the model uncertainty description as it will be shown in the next subsection. The considered device has an input current limitation of ± 1 A which corresponds to the range of allowed yaw moment values (i.e. ± 2500 Nm) that can be mechanically generated.

3.3. Model uncertainty description

On the basis of the vehicle and actuator descriptions introduced in Sections 3.1 and 3.2 plant dynamics can be characterized for control purposes by the following model:

$$G_{Plant}(s) = G_A(s)G_M(s) = G(s)e^{-\vartheta_A s}, \quad (7)$$

where $G(s) = G_A'(s)G_M(s)$ (see (3) and (6)). Model (7) is computed for suitable values of the vehicle and actuator parameters to define a nominal operating condition to be employed in the controller design. However, to take into account the wide range of the vehicle manoeuvring situations an appropriate uncertainty description has to be introduced. To this end, an additive model set of the form (8) (see e.g. Milanese & Taragna, 2005) has been identified on the basis of the minimum phase part $G(s)$ of the nominal model (7) and simulated data generated by means of an accurate 14 degrees of freedom vehicle model:

$$\mathcal{G}(G, \Gamma(\omega)) = \{G(s) + \Delta(s) : |\Delta(\omega)| \leq \Gamma(\omega)\}. \quad (8)$$

In model set (8) $G(s)$ is the nominal transfer function between the control variable (i.e. I_M) and the vehicle yaw rate, $\Delta(s)$ is the unstructured additive uncertainty and $\Gamma(\omega)$ is an upper bound of the magnitude of $\Delta(s)$. The data employed in the identification of the uncertainty have been obtained taking into account the effects of different tyre characteristics ($\pm 10\%$ front, $\pm 10\%$ rear tyre cornering stiffness and $\pm 10\%$ tyre relaxation lengths variations with respect to their nominal values), vehicle speeds ($\pm 30\%$ of the nominal value), vehicle mass (0% to +25% of the nominal value with consequent geometrical and inertial parameters changes). Effects of variable delays (up to 5 ms) in yaw moment generation induced by mechanical components other than the hydraulic valves have been included

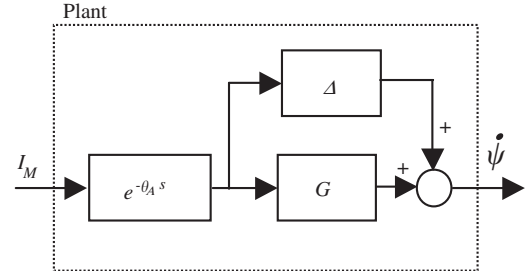


Fig. 5. Plant model scheme.

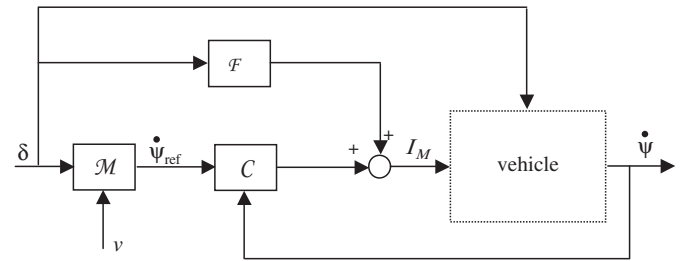


Fig. 6. Control structure schematic.

too. In Fig. 5, a schematic of the model set used to describe the system dynamics and employed in the controller design is reported. The course of the computed model set defined in (8) is shown in Fig. 14 of Section 5.

4. Yaw control using IMC

A functional scheme of the considered control structure is depicted in Fig. 6. In such a structure the desired yaw rate behaviour is imposed by the yaw rate reference signal $\dot{\psi}_{ref}(t)$ which is generated by a static map \mathcal{M} using the values of $\delta(t)$ and $v(t)$. The feedback controller \mathcal{C} computes the input current contribution needed to follow the required yaw rate performances described by $\dot{\psi}_{ref}(t)$. Moreover, in order to improve the yaw rate transient response properties in face of the driver input, a feedforward contribution \mathcal{F} from $\delta(t)$ has been added too.

4.1. Reference generator

Reference yaw rate values are generated using a non-linear static map

$$\dot{\psi}_{ref} = f(\delta, v) \quad (9)$$

which uses as inputs the front steering angle δ imposed by the driver and the vehicle speed v . The values of $f(\delta, v)$ are generated according to the control objective, i.e. to improve the vehicle understeering curve, in terms of vehicle manoeuvrability and lateral acceleration limit, thus enhancing the overall vehicle handling quality perceived by the driver (see Data & Frigerio, 2002). In order to compute the map values, a single track non-linear steady state vehicle model is considered. This model differs from the one presented in Section 3 by the fact that it considers steady

state vehicle behaviour only and it takes into account a non-linear static axle slip–lateral force relationship, given by the following equation introduced in Bakker et al. (1989):

$$F_{y,p}(\alpha, F_z) = D(C \arctan(B(\alpha + S_h) - E(B(\alpha + S_h) - \arctan(B(\alpha + S_h)))))) + S_v, \quad (10)$$

where F_z is the vertical load applied on the tyre and α is the tyre sideslip angle. B , C , D , E , S_h , S_v are parameters which depend on F_z as follows:

$$B(F_z) = \frac{p_3 \sin(2 \arctan(F_z/p_4))}{C(F_z)D(F_z)},$$

$$C(F_z) = p_{00} + p_{01}F_z,$$

$$D(F_z) = p_1 F_z^2 + p_2 F_z,$$

$$E(F_z) = p_6 F_z + p_7,$$

$$S_h(F_z) = p_9 F_z + p_{10},$$

$$S_v(F_z) = p_{12} F_z + p_{13}, \quad (11)$$

where parameters p_{00} , p_{01} , p_1 , p_2 , p_3 , p_4 , p_6 , p_7 , p_9 , p_{10} , p_{12} and p_{13} can be identified, for a given uncontrolled vehicle, using the experimental data collected during standard handling manoeuvres (see e.g. Vetturi, Gadola, Manzo, & Faglia, 1996).

In the single track model, front and rear axle tyre sideslip angles can be written as

$$\alpha_f(t) = \beta(t) + a\dot{\psi}(t)/v(t) - \delta(t),$$

$$\alpha_r(t) = \beta(t) - b\dot{\psi}(t)/v(t) \quad (12)$$

as a consequence, front and rear axle tyre lateral forces can be expressed as functions of β , $\dot{\psi}$, δ and of the vertical loads $F_{zf,p}$ and $F_{zr,p}$ applied on the front and rear axle, respectively, which can be computed as

$$F_{zf,p} = bmg/l,$$

$$F_{zr,p} = amg/l, \quad (13)$$

where g is the gravity acceleration. Consider now the first two equations of (2): in steady state conditions (i.e. $\dot{\psi} = 0$, $\dot{\beta} = 0$) they can be rewritten as

$$mv\dot{\psi} = F_{yf,p} + F_{yr,p},$$

$$aF_{yf,p} - bF_{yr,p} + M_z = 0 \quad (14)$$

then, by replacing $F_{yf,p}$, $F_{yr,p}$ in (14) with the corresponding expressions obtained from Eqs. (10) to (13) and considering the steady state equation $M_z = \bar{K}_A K_A I_M$, obtained from (6), the single track steady state non-linear model equations can be obtained:

$$mv\dot{\psi} = F_{yf,p}(\beta, \dot{\psi}, \delta, F_{zf}) + F_{yr,p}(\beta, \dot{\psi}, F_{zr}),$$

$$aF_{yf,p}(\beta, \dot{\psi}, \delta, F_{zf}) - bF_{yr,p}(\beta, \dot{\psi}, F_{zr}) + \bar{K}_A K_A I_M = 0. \quad (15)$$

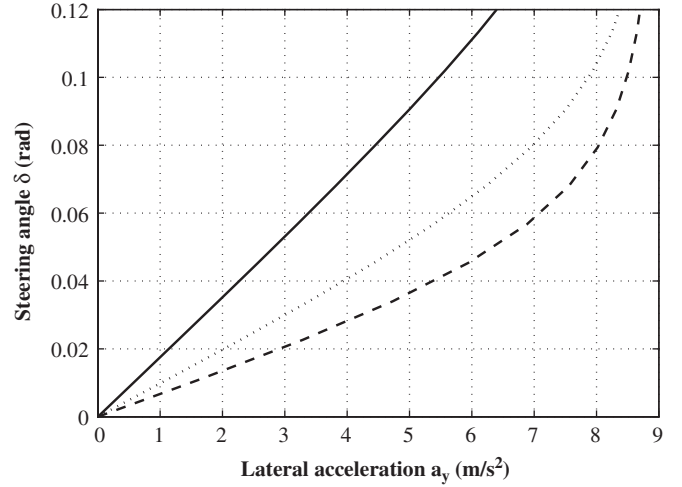


Fig. 7. Uncontrolled vehicle understeering curves at 50 km/h (solid), 80 km/h (dotted) and 130 km/h (dashed).

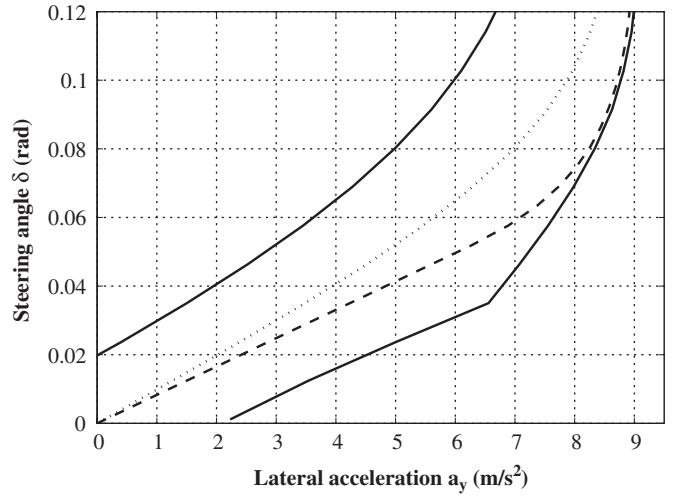


Fig. 8. Control system working zone, delimited by solid lines, and uncontrolled (dotted) and reference (dashed) vehicle understeering curves. Speed: 80 km/h.

This non-linear model is employed in a two-step procedure to compute the reference map values. First of all, Eqs. (15) are used to compute the uncontrolled car understeering curve at each constant speed value (see Fig. 7) and any possible controlled vehicle understeering curve, within the vehicle lateral acceleration limit, obtained applying every manipulated variable value inside the saturation limits of the actuator (i.e. $|I_M| \leq 1$ A) for each couple of values (δ, v) . Thus, for each constant speed value, the working region for the control system can be obtained (see Fig. 8, solid lines). This region represents a limit to the reference understeering curve that can be set for the controlled vehicle with the nominal tyre, mass and geometrical characteristics.

In the second step, the reference understeering curve at each speed value is chosen within the working region according to some performance criteria. To this end, the curve can be divided into a linear tract (i.e. small lateral

acceleration values) and into a non-linear one. In the first tract, a commonly employed performance criterium is to improve the vehicle manoeuvrability by reducing the slope of the curve. In the non-linear tract, a trade off has to be chosen: on the one hand, it is suitable to modify the non-linear part of the curve in order to increase the lateral acceleration range for which the controlled vehicle understeering characteristic behaves linearly (see e.g. Fig. 9, dashed line); on the other hand, it is also necessary a smooth connection of the linear tract with the maximum lateral acceleration value (as reported in Fig. 9, dotted line), to avoid the driver to suddenly feel that the car has reached its cornering limit, after which a steering angle increment does not correspond to a lateral acceleration increment (i.e. the cornering radius cannot be shortened by means of a simple steering action), thus likely giving place to critical driving situations. Finally, with the considered actuator it is possible to slightly increase the maximum lateral acceleration that the vehicle can reach, which corresponds to an improvement of its handling and safety characteristics. From a practical point of view, the two understeering curves reported in Fig. 9 can be associated to different vehicle handling features. In particular, the dashed line corresponds to a quite sportive car behaviour while the dotted course is related to more quiet vehicle cornering characteristics.

In the linear tract of the understeering curve, the uncontrolled car behaviour can be expressed as

$$\delta = \left(\frac{l}{v^2} + K_V\right) a_y = \left(\frac{l}{v} + K_V v\right) \dot{\psi}. \quad (16)$$

The quantity K_V is the vehicle *understeering gradient*, which is defined as (see Rajamani, 2005):

$$K_V = \frac{m}{l} \left(\frac{b}{c_f} - \frac{a}{c_r}\right). \quad (17)$$

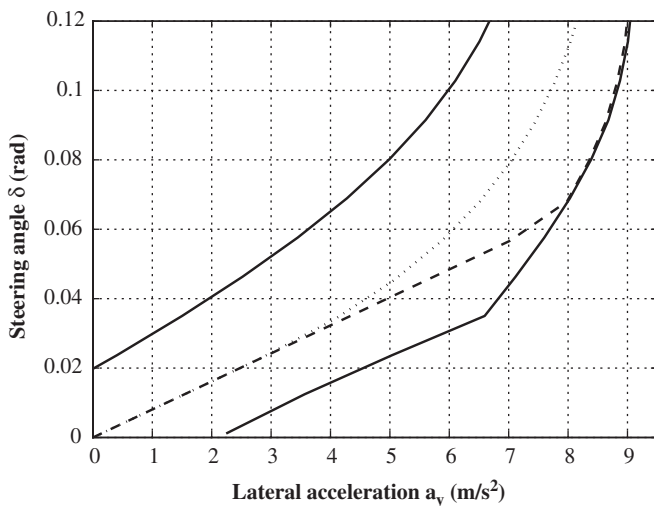


Fig. 9. Different possible reference understeering curve choices for the non-linear tract and control system working zone (solid). Speed: 80 km/h.

Eq. (17) is obtained considering the cornering stiffness for the overall front (rear) axle instead of the single front (rear) wheels. Since the perceived handling quality of a vehicle with a lower understeering gradient is higher, reference curves in the linear tract are chosen in order to decrease the factor K_V . The desired (reference) car yaw rate $\dot{\psi}_{ref}$ and lateral acceleration $a_{y,ref}$ in the linear tract are therefore imposed as

$$\begin{aligned} \delta &= \left(\frac{l}{v^2} + K_C\right) a_{y,ref} \\ &= \left(\frac{l}{v} + K_C v\right) \dot{\psi}_{ref} \quad \text{for } 0 \leq v \dot{\psi}_{ref} \leq a_{y,l} \end{aligned} \quad (18)$$

with $K_C < K_V$. The term $a_{y,l}$ is an arbitrary lateral acceleration value which limits the linear tract of the controlled vehicle reference behaviour: starting from this value, the desired understeering curve is computed considering the following logarithmic relationship:

$$\begin{aligned} \delta &= \delta_{l,v} - \left(\frac{l}{v^2} + K_C\right) (\bar{a}_y - a_{y,l}) \ln\left(\frac{\bar{a}_y - a_{y,ref}}{\bar{a}_y - a_{y,l}}\right) \\ &= \delta_{l,v} - \left(\frac{l}{v^2} + K_C\right) (\bar{a}_y - a_{y,l}) \\ &\quad \times \ln\left(\frac{\bar{a}_y - v \dot{\psi}_{ref}}{\bar{a}_y - a_{y,l}}\right) \quad \text{for } a_{y,l} < v \dot{\psi}_{ref} < \bar{a}_y, \end{aligned} \quad (19)$$

where $\delta_{l,v}$ is the front steering angle value which corresponds to lateral acceleration $a_{y,l}$ at each vehicle speed value v . The form of Eq. (19) has been chosen to perform a smooth connection between the linear tract of the curve and the maximum lateral acceleration value \bar{a}_y . The value of $a_{y,l}$ can be chosen to increase the range of lateral acceleration values which corresponds to the linear tract of the controlled vehicle understeering curve. The value of \bar{a}_y is selected as the maximum lateral acceleration that the controlled vehicle can reach, without violating the physical upper bound suggested by Rajamani (2005):

$$\bar{a}_y \leq 0.85\mu, \quad (20)$$

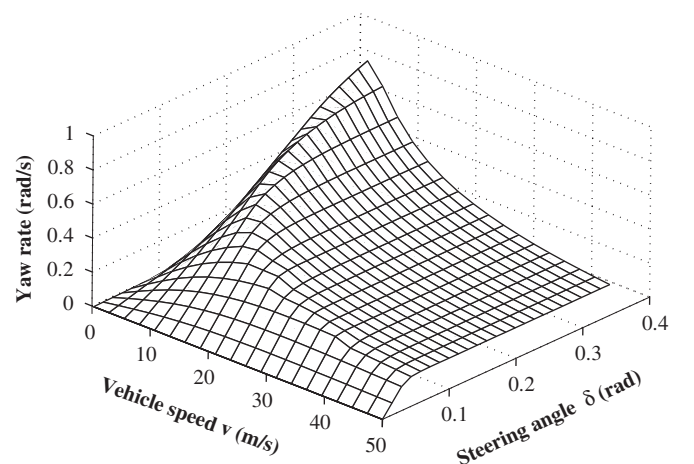


Fig. 10. An example of yaw rate reference static map.

where μ is the available tyre-road friction. Eqs. (18) and (19) give the reference yaw rate value for each couple of values of δ and v , so a map of values of $\dot{\psi}_{ref}(\delta, v)$ is computed. Fig. 10 shows an example of such a static reference map. For negative values of δ , the symmetric map with respect to the reference yaw rate obtained for positive δ values is considered.

4.2. Feedback controller design

The feedback controller has a twofold objective: guarantee robust stability in face of input saturation given by the RAD device and optimize the performances when such saturation is active. IMC approaches (see Morari & Zafriou, 1989) based on H_∞ optimization are able to satisfy robust stability requirements in presence of input saturation (see e.g. Canale, 2004; Malan, Milanese, Regruto, & Taragna, 2004). A basic IMC scheme is reported in Fig. 11. However, as discussed in Goodwin et al. (1993), Zheng et al. (1994), IMC control may deteriorate the system performances when saturation is active even in absence of model uncertainty. In order to improve the performances under saturation an enhanced robust IMC structure based on the anti-windup IMC solutions presented in Goodwin et al. (1993), Zheng et al. (1994) has been proposed in Canale (2004). The control scheme considered in Canale (2004) gives rise to a non-linear controller \mathcal{Q} which replaces the linear controller $Q(s)$ in Fig. 11 made up by the cascade

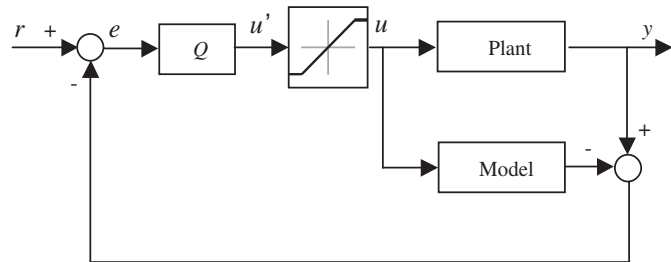


Fig. 11. IMC basic scheme.

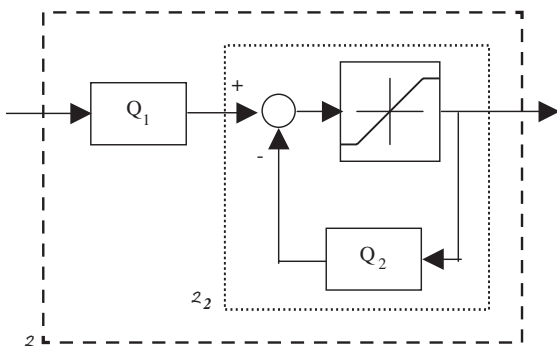


Fig. 12. Non-linear IMC enhanced controller.

connection of a linear filter $Q_1(s)$ and a non-linear loop \mathcal{Q}_2 as shown in Fig. 12.

In linear operating conditions (i.e. when the saturation is not active) the improved IMC structure is equivalent to a “standard” IMC controller of the form:

$$Q_{eq}(s) = \frac{Q_1(s)}{1 + Q_2(s)} \tag{21}$$

The design procedure can be summarized in the following steps:

- (1) A preliminary robust IMC controller $Q(s)$ is computed solving the following optimization problem:

$$Q(s) = \arg \min_{\|Q(s)\bar{F}(s)\|_\infty < 1} \|W_S^{-1}(s)(1 - G(s)Q(s))\|_\infty, \tag{22}$$

where $\bar{F}(s)$ is suitable rational function with real coefficients, stable, whose magnitude strictly overbounds the frequency behaviour $\Gamma(\omega)$ and $W_S(s)$ is a weighting function introduced to take into account a desired specification on the behaviour of the nominal

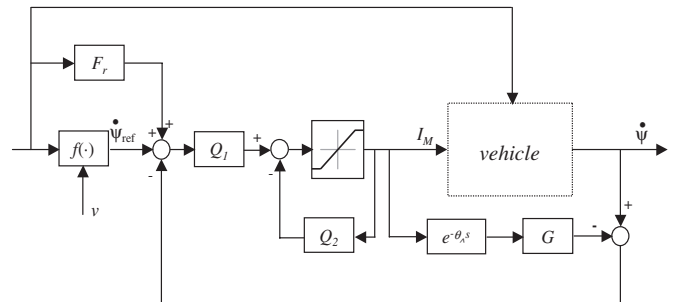


Fig. 13. The proposed control scheme.

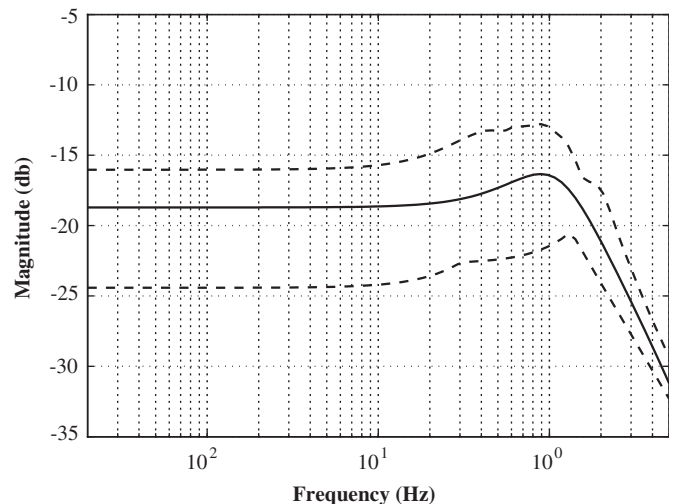


Fig. 14. Model set \mathcal{G} : nominal transfer function G (solid) and upper and lower uncertainty bounds (dashed).

sensitivity $S(s) = 1 - G(s)Q(s)$. Note that, according to well established design procedure in IMC context (see e.g. Morari & Zafriou, 1989), only the minimum phase part $G(s)$ has been used in the controller computation. However, delay has been taken into account in the model prediction path of the controller (see Fig. 13).

- (2) Using controller $Q(s)$ computed in the previous step, a controller $Q_2(s)$, via the design of a preliminary filter $\bar{Q}_1(s)$, is obtained according to the criteria introduced in Goodwin et al. (1993) and Zheng et al. (1994). It has to be noted that $Q_2(s)$ must ensure the stability of the non-linear loop \mathcal{Q}_2 (see Fig. 12). To this end, an upper bound $\gamma_{\mathcal{Q}_2}$ on the H_∞ norm of \mathcal{Q}_2 has to be computed (see Canale, 2004 for details). If $\gamma_{\mathcal{Q}_2}$ is finite then the stability of \mathcal{Q}_2 is guaranteed. In case that the stability of \mathcal{Q}_2 is not assured then a new controller design has to be

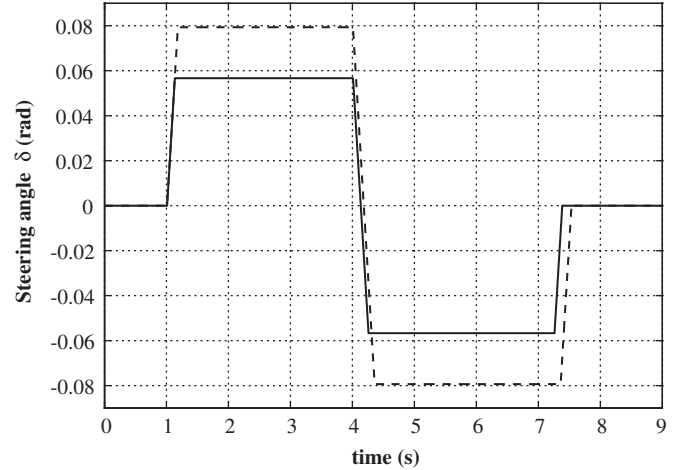


Fig. 15. Steering angle reversal test inputs corresponding to 70° (dashed) and 50° (solid) handwheel angle.

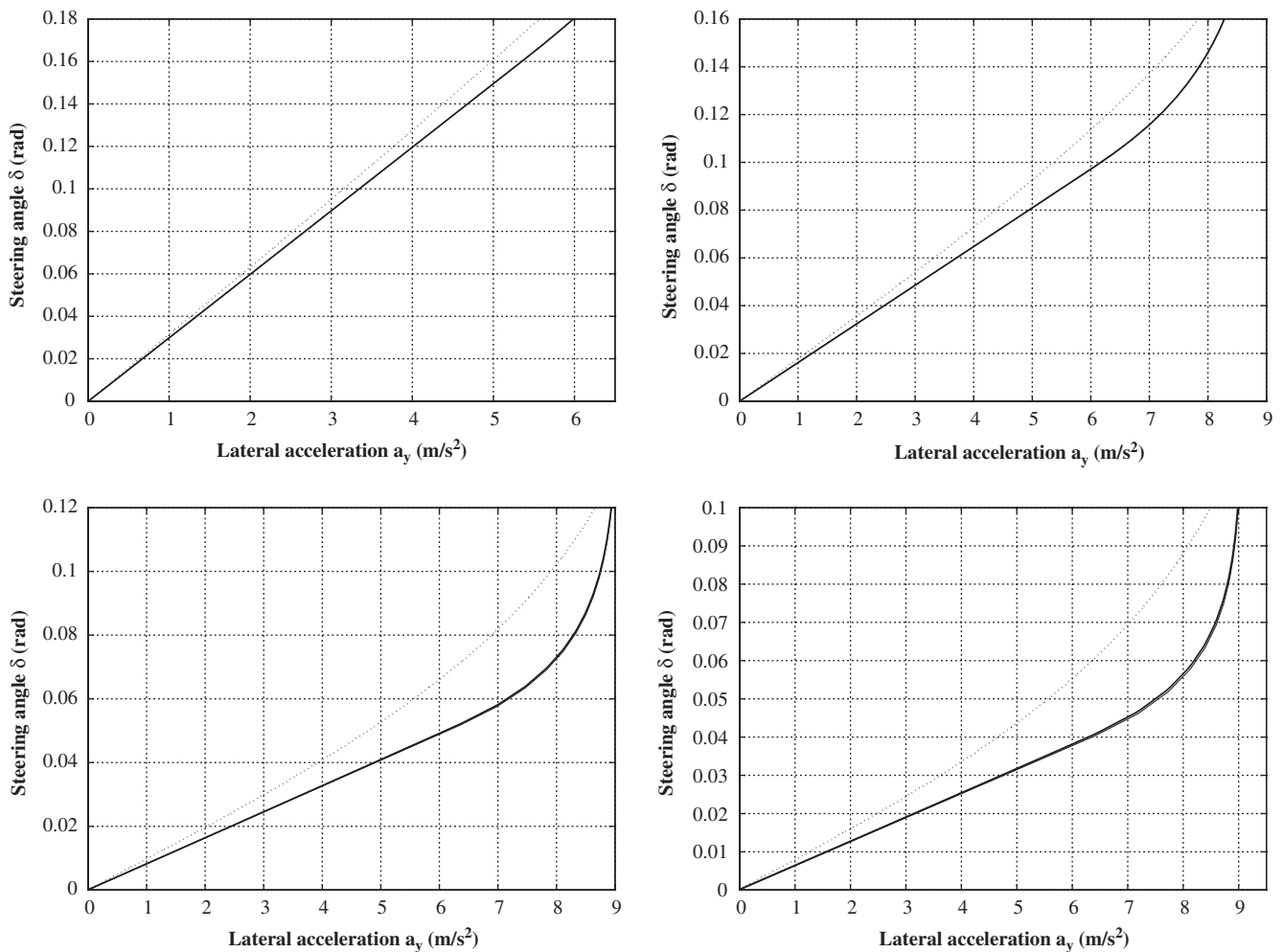


Fig. 16. Light mass vehicle: comparison between the reference (thin solid line) understeering curve for steering pad manoeuvres at constant speed and the ones obtained for the uncontrolled vehicle (dotted) and for the controlled vehicle (solid). Vehicle speeds: 35 km/h (upper left), 50 km/h (upper right), 80 km/h (lower left), 100 km/h (lower right).

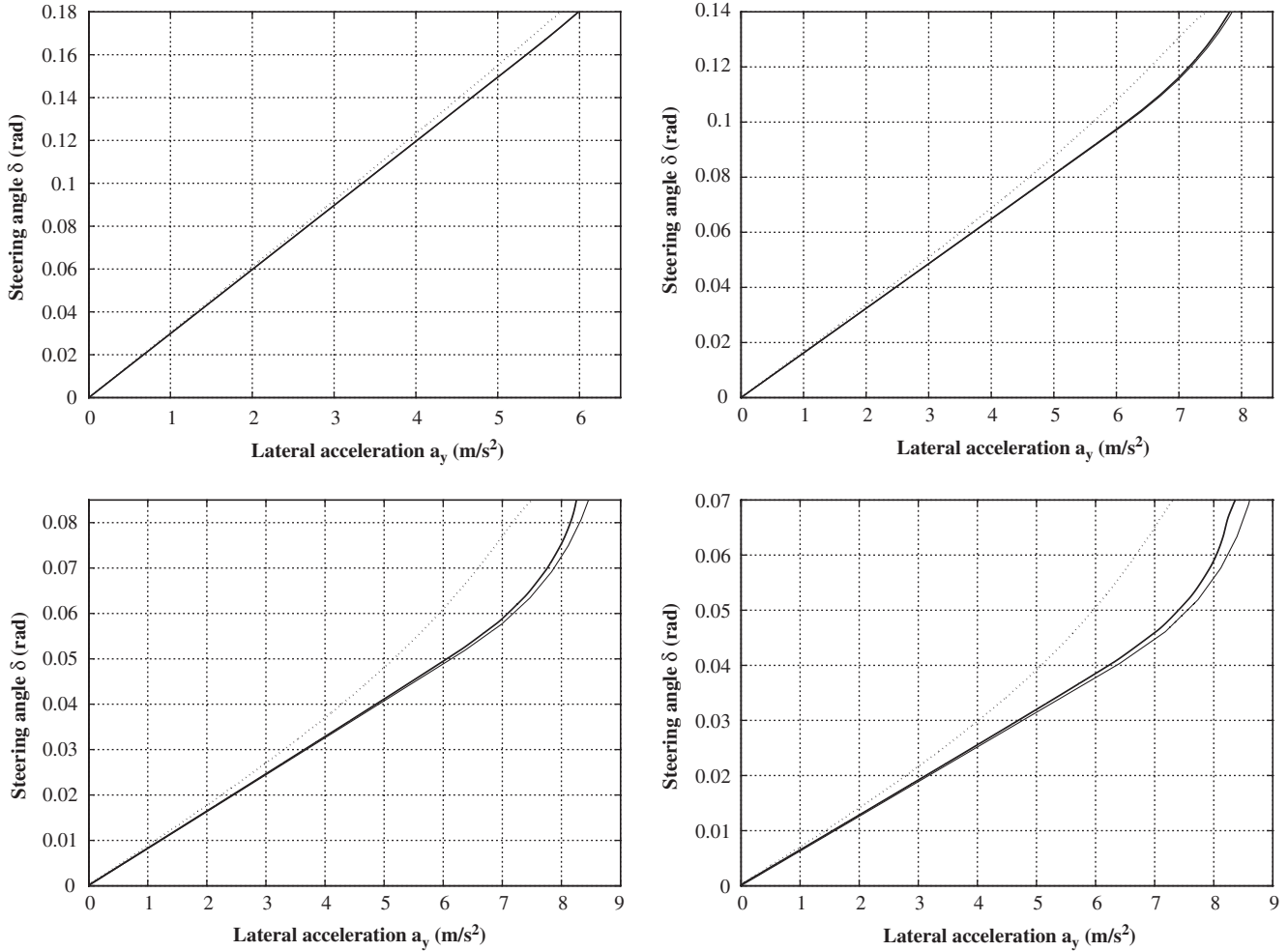


Fig. 17. Full load vehicle: comparison between the reference (thin solid line) understeering curve for steering pad manoeuvres at constant speed and the ones obtained for the uncontrolled vehicle (dotted) and for the controlled vehicle (solid). Vehicle speeds: 35 km/h (upper left), 50 km/h (upper right), 80 km/h (lower left), 100 km/h (lower right).

performed (i.e. starting from point (1) of the procedure).

(3) Then, the linear controller $Q_1(s)$ can be designed by means of the following H_∞ optimization problem:

$$Q_1(s) = \arg \min_{\|Q_1(s)F(s)\|_{\infty} < 1} \left\| W_S^{-1}(s) \left(1 - G(s) \frac{Q_1(s)}{1 + Q_2(s)} \right) \right\|_{\infty} \quad (23)$$

4.3. Feedforward controller design

In order to improve the yaw rate transient response a further control input generated by a feedforward controller driven by the steering angle $\delta(t)$ is added. Such a feedforward yaw moment contribution is computed by means of a linear filter $F(s)$ to match the open loop yaw rate behaviour given by (3) with the one described by an

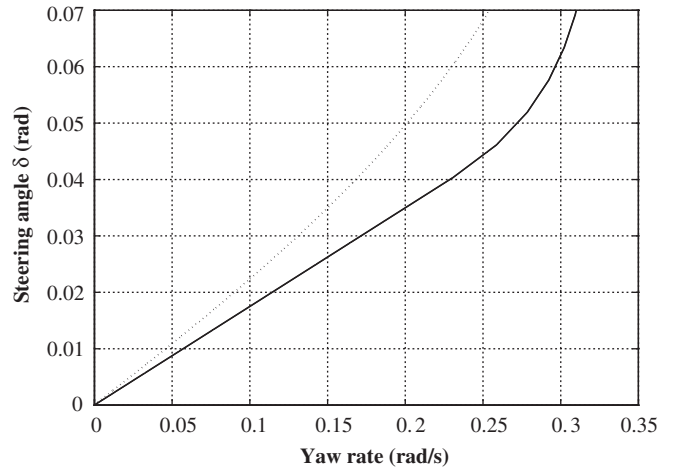


Fig. 18. Full load vehicle: yaw rate reference (thin solid line) understeering curve for steering pad manoeuvre at 100 km/h and simulation results for the uncontrolled vehicle (dotted) and for the controlled one (solid).

objective transfer function $T_{\delta}^{des}(s)$:

$$\dot{\psi}(s) = T_{\delta}^{des}(s)\delta(s). \quad (24)$$

Thus, considering relations (3), (6) and (7) where $I_M(s)$ is computed as $I_M(s) = F(s)\delta(s)$ and $\dot{\psi}(s)$ is given by (24), the feedforward filter $F(s)$ is derived as

$$F(s) = \frac{T_{\delta}^{des}(s) - G_{\delta}(s)}{G(s)}. \quad (25)$$

The transfer function $T_{\delta}^{des}(s)$ can be chosen as a first or second order function. Moreover, as the feedforward controller aims to enhance the transient response only, its contribution should be deactivated in steady state conditions. This is achieved when the dc-gains of $T_{\delta}^{des}(s)$ and $G_{\delta}(s)$ are the same.

It has to be noted that if such feedforward action would be implemented as shown in Fig. 6, the improvements introduced during saturation by the structure of Fig. 12 will influence only the feedback control contribution. This may cause a slight degradation on the control performances. In order to avoid such a degradation, the

feedforward contribution will be injected at the reference level obtaining the control scheme reported in Fig. 13.

In such a structure the feedforward action is realized by the linear filter $F_r(s)$, whose expression can be computed by straightforward manipulations as

$$F_r(s) = \left(\frac{1 + Q_2(s)}{Q_1(s)} - G(s) \right) F(s). \quad (26)$$

5. Simulation results

The control design has been performed using transfer functions $G_{\delta}(s)$ and $G(s)$ defined in (4), (5), (6) and (7) computed at a nominal speed $v = 100 \text{ km/h} = 27.77 \text{ m/s}$ and with the following values of the other involved parameters:

- $m = 1715 \text{ kg}$, $J_z = 2700 \text{ kgm}^2$,
- $a = 1.07 \text{ m}$, $b = 1.47 \text{ m}$,
- $l_f = 1 \text{ m}$, $l_r = 1 \text{ m}$,
- $c_f = 95117 \text{ Nm/rad}$, $c_r = 97556 \text{ Nm/rad}$,
- $\omega_A = 53.4 \text{ rad/s}$, $\vartheta_A = 20 \text{ ms}$,
- $K_A = 5 \text{ bar/A}$, $\bar{K}_A = 500 \text{ Nm/bar}$.

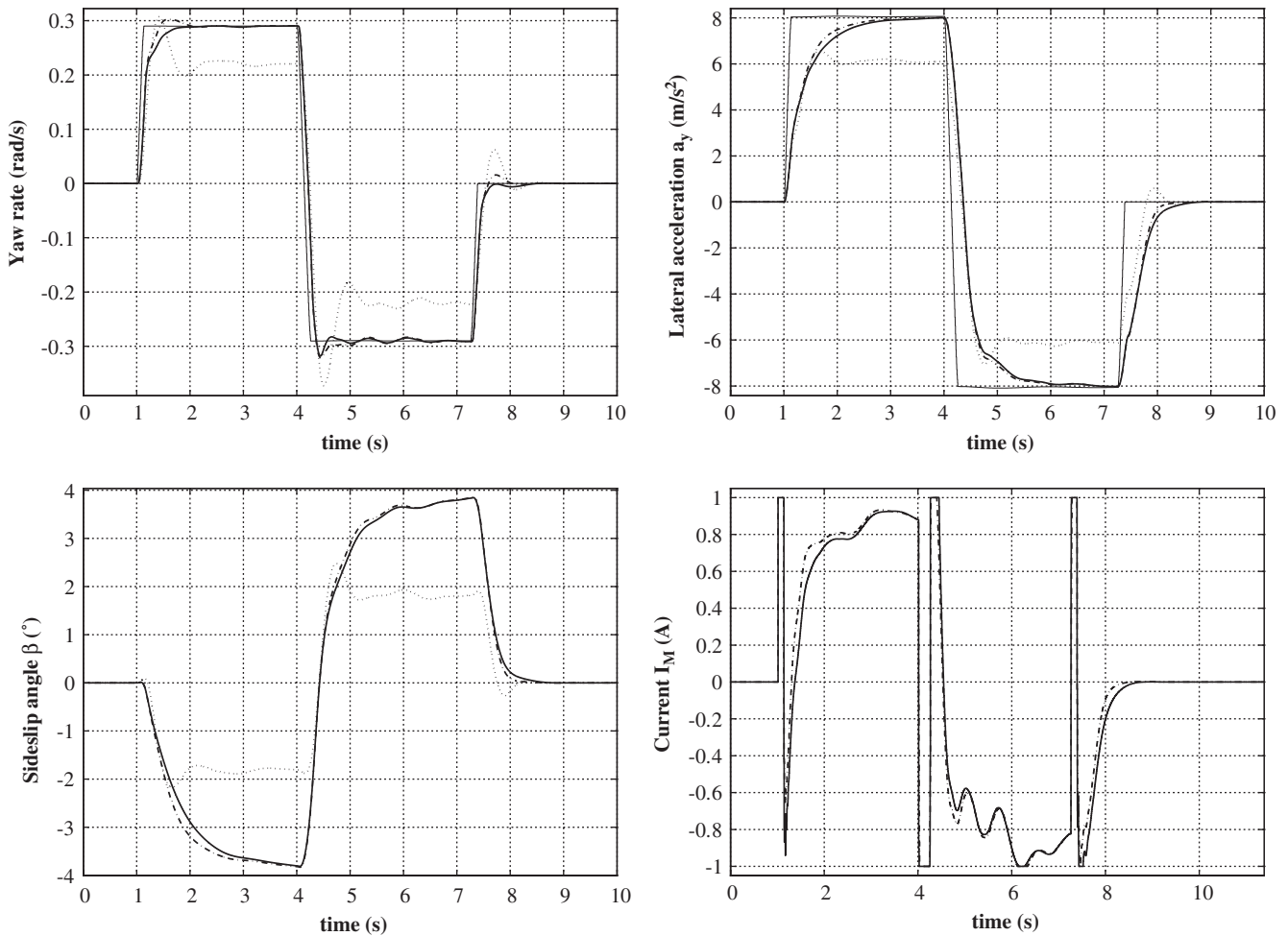


Fig. 19. Light mass vehicle, steer reversal test: vehicle speed: 100 km/h. Handwheel value: 50°. Comparison between the reference (thin solid line), uncontrolled (dotted), basic IMC (dash-dot) and enhanced IMC (solid) controlled vehicle behaviour.

The computed model set (8) is shown in Fig. 14 where the nominal transfer function magnitude behaviour is reported and compared with the obtained uncertainty bounds. The following weighting function $W_S(s)$ has been used in the optimization problem (22):

$$W_S(s) = 1.12 \frac{s}{s + 20} \quad (27)$$

The following controller $Q(s)$ has been computed:

$$Q(s) = 178.08 \frac{(s + 51.42)(s^2 + 9.03s + 49.14)}{(s + 116.51)(s + 81.78)(s + 5.48)} \quad (28)$$

The preliminary filter $\bar{Q}_1(s)$ has been chosen as $\bar{Q}_1(s) = G_f(s)Q(s)G_M(s)$ (see, Zheng et al., 1994), giving rise to the following expression for $Q_2(s)$:

$$Q_2(s) = G_f(s)G_M(s) - 1. \quad (29)$$

In order to obtain a strictly proper expression for $Q_2(s)$ (as required for implementation), $G_f(s)$ has been chosen of the form:

$$G_f(s) = K_G(s + \omega_{z,1})(s + \omega_{z,2}), \quad (30)$$

where K_G is the inverse of the gain of $G(s)$ (i.e. $K_G = a_4/(c_3\bar{K}_A K_A \omega_A)$), see (4), (5) and (6). Thus, the

preliminary filter $\bar{Q}_1(s)$ contains two design parameters, $\omega_{z,1}$ and $\omega_{z,2}$, whose values have to be chosen to obtain a good compromise between robust stability and nominal performances: the higher $\omega_{z,1}$ and $\omega_{z,2}$, the better the system performances obtained at the expense of robustness. The chosen values are $\omega_{z,1} = 6$ rad/s and $\omega_{z,2} = 120$ rad/s; the corresponding value of $\gamma_{\mathcal{L}_2}$ is equal to 0 dB. On the basis of such choices, the following linear controller $Q_1(s)$ has been computed according to the optimization problem (23):

$$Q_1(s) = 463.94 \frac{(s + 120)(s + 5.99)}{(s + 253.21)(s + 90.65)} \quad (31)$$

Finally, as regards the feedforward design, the transfer function $T_\delta^{des}(s)$ has been chosen as

$$T_\delta^{des}(s) = \frac{16157.34}{(s + 600)(s + 6)}$$

In order to show in a realistic way the performances obtained by the proposed yaw control approach, the controller has been discretized with a sampling time equal to 5 ms (which corresponds to the real system ECU main task sampling time) and simulations have been performed

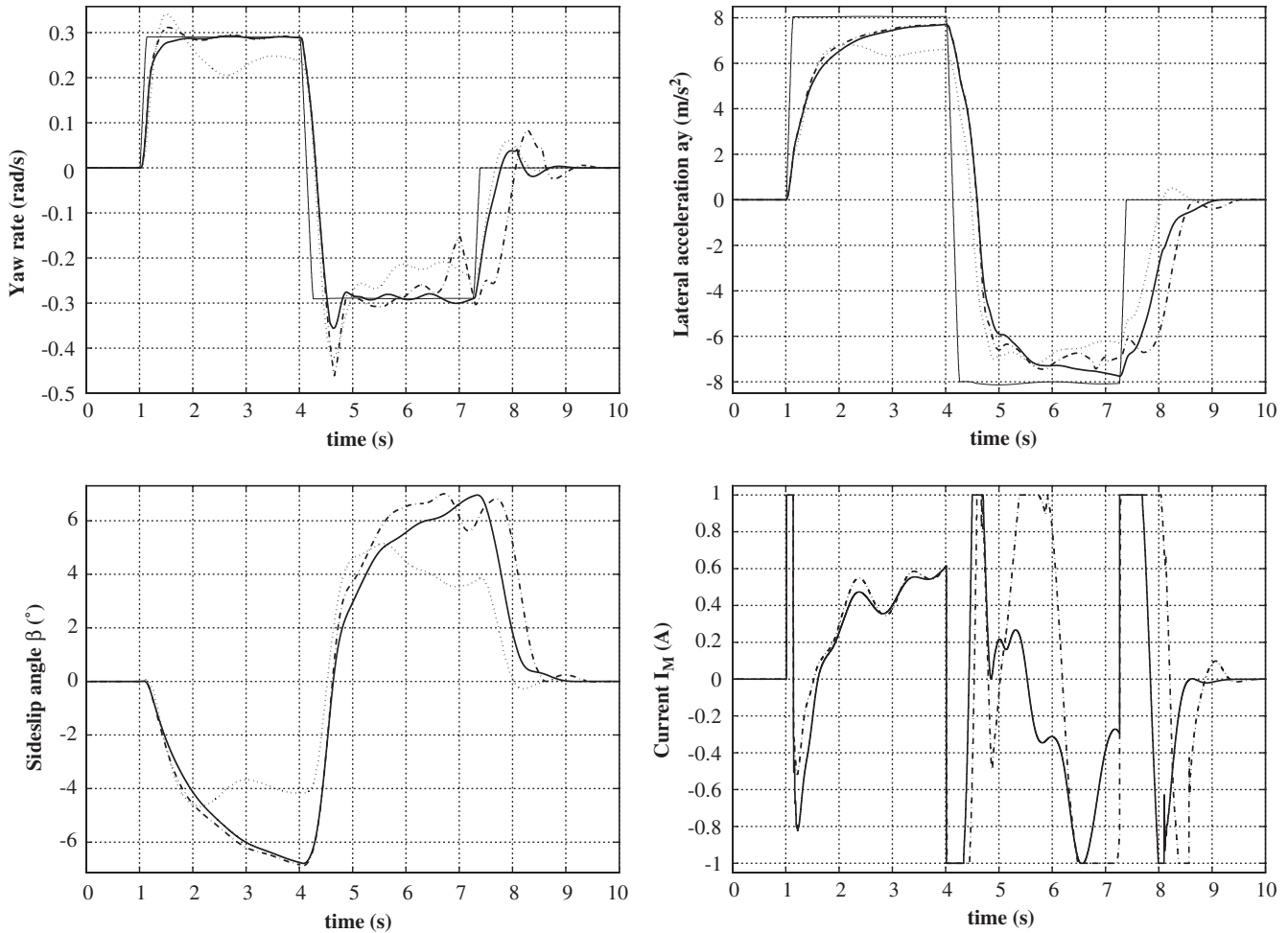


Fig. 20. Full load vehicle, steer reversal test: vehicle speed: 100 km/h. Handwheel value: 50°. Comparison between the reference (thin solid line), uncontrolled (dotted), basic IMC (dash-dot) and enhanced IMC (solid) controlled vehicle behaviour.

using a detailed non-linear 14 degrees of freedom Simulink model which proved to give an accurate description of the vehicle dynamics as compared to actual measurements (see Colombo, 2005). In particular, the model degrees of freedom correspond to the standard three chassis translations and yaw, pitch and roll angles, the four wheel angular speeds and the four wheel vertical movements with respect to the chassis. Non-linear characteristics obtained on the basis of measurements on the real vehicle have been employed to model the tyre, steer and suspension behaviour.

In order to highlight the controlled car safety, as well as steady state and transient handling performances, and to compare these characteristics with the uncontrolled vehicle and with the basic IMC system ones, the following open loop (i.e. without driver's feedback) manoeuvres have been chosen:

- constant speed steering pad performed at 35, 50, 80 and 100 km/h: the steering angle is increased at the rate of $1^\circ/\text{s}$ while the vehicle is moving at constant speed, until the vehicle lateral acceleration limit is reached;
 - steer reversal tests with handwheel angle of 50° and 70° performed at 100 and 70 km/h, respectively, with a steering wheel speed of $400^\circ/\text{s}$. These tests aim to evaluate the controlled car transient and steady state performances: in Fig. 15 the employed steering angle time histories are showed.
 - μ -split braking manoeuvre performed at 80 km/h with dry road on one side and icy road on the other, with braking pedal input corresponding to a deceleration value of 0.5 g on dry road.
 - steering wheel frequency sweep performed at 100 km/h in the frequency range 0–3 Hz with steering wheel angle amplitude of 20° .
- All such manoeuvres have been performed with two vehicle mass values (and consequent geometrical and inertial parameters changes): 1715 kg (light mass) and 2100 kg (full load).
- Handwheel step input of 50° performed at 80 km/h, with a handwheel speed of $400^\circ/\text{s}$, and lateral wind disturbance step during the cornering, with 100 km/h wind speed. The wind disturbance occurs after the transient phase of the reference step input has been completed.

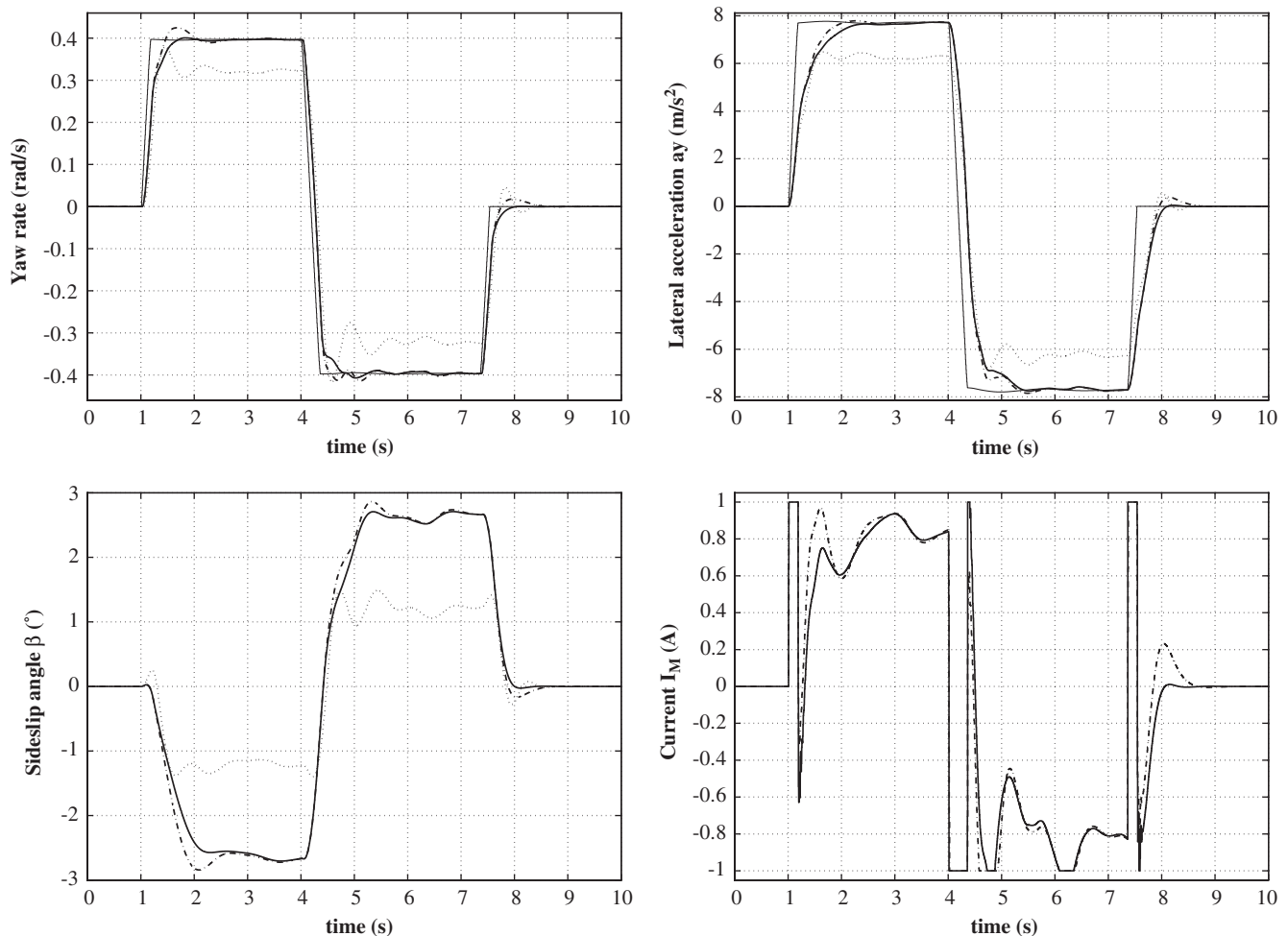


Fig. 21. Light mass vehicle, steer reversal test: vehicle speed: 70 km/h. Handwheel value: 70° . Comparison between the reference (thin solid line), uncontrolled (dotted), basic IMC (dash-dot) and enhanced IMC (solid) controlled vehicle behaviour.

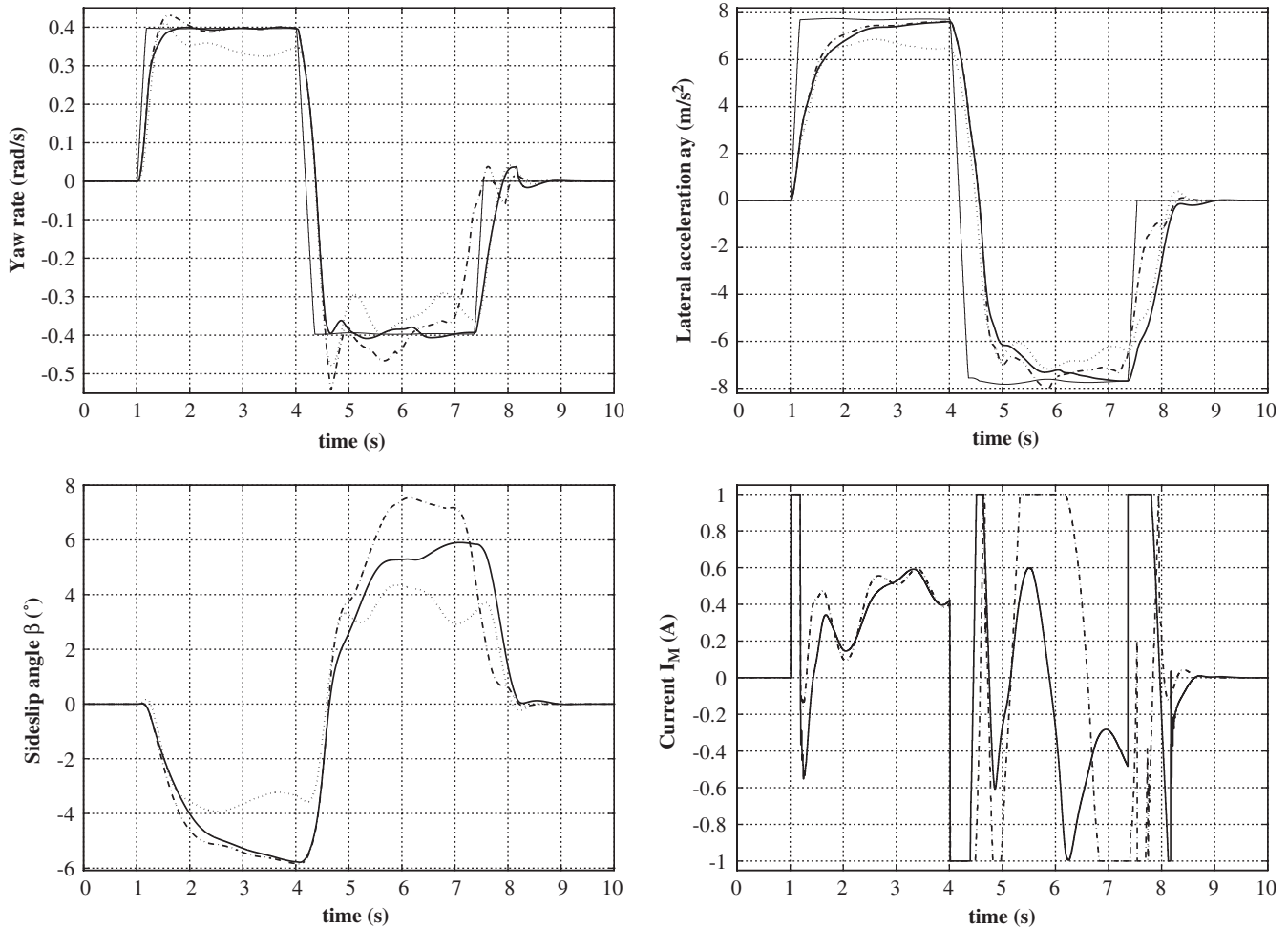


Fig. 22. Full load vehicle, steer reversal test: vehicle speed: 70 km/h. Handwheel value: 70°. Comparison between the reference (thin solid line), uncontrolled (dotted), basic IMC (dash-dot) and enhanced IMC (solid) controlled vehicle behaviour.

In this test, vehicle mass was increased by 15%, with consequently changed inertial and geometrical vehicle characteristics, and low friction road conditions have been considered, with $\mu = 0.7$ (wet road). The purpose of this test is to evaluate the control system robustness in a quite demanding way in front of external disturbances and parameter variations.

In Figs. 16 and 17 the understeering performance improvement is showed for the considered steering pad manoeuvres. As it can be noted, the target vehicle behaviour in the linear zone, characterized by a lower understeering gradient, is reached for both vehicle load configurations and for every considered speed value (see the superimposed courses of the solid lines). The basic IMC scheme (i.e. without anti-windup structure) and the one proposed in this paper have the same steady state performance, thus only the enhanced IMC results are showed. The difference between light mass and full load uncontrolled vehicle behaviour becomes more evident as vehicle speed increases. In particular, the controlled car behaviour is always the same within the linear tract of the

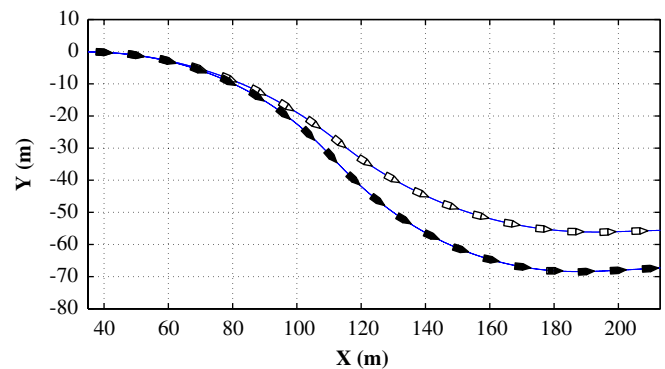


Fig. 23. Light mass vehicle: uncontrolled (white) and controlled (black) vehicle paths for steer reversal test at 100 km/h with 50° handwheel.

curve and remains very close to the desired performances also in the non-linear zone. A small difference with respect to the reference value for the full load vehicle at very high lateral acceleration values occurs due to the fact that the vehicle does not reach steady state conditions because of its increased inertial characteristics. In fact, the reference lateral acceleration value is computed as $a_{y,\text{ref}} = \dot{\psi}_{y,\text{ref}}v$,

which is accurate only in steady state conditions. However, the yaw rate reference is perfectly followed as witnessed by Fig. 18, which shows the yaw rate understeering curve obtained in the 100 km/h steering pad manoeuvre.

The 50° steer reversal tests at 100 km/h allow to study the results obtained when the vehicle reaches the lateral acceleration limit of about 8 m/s² (see Figs. 19 and 20). Control system is able to reach the reference yaw rate value

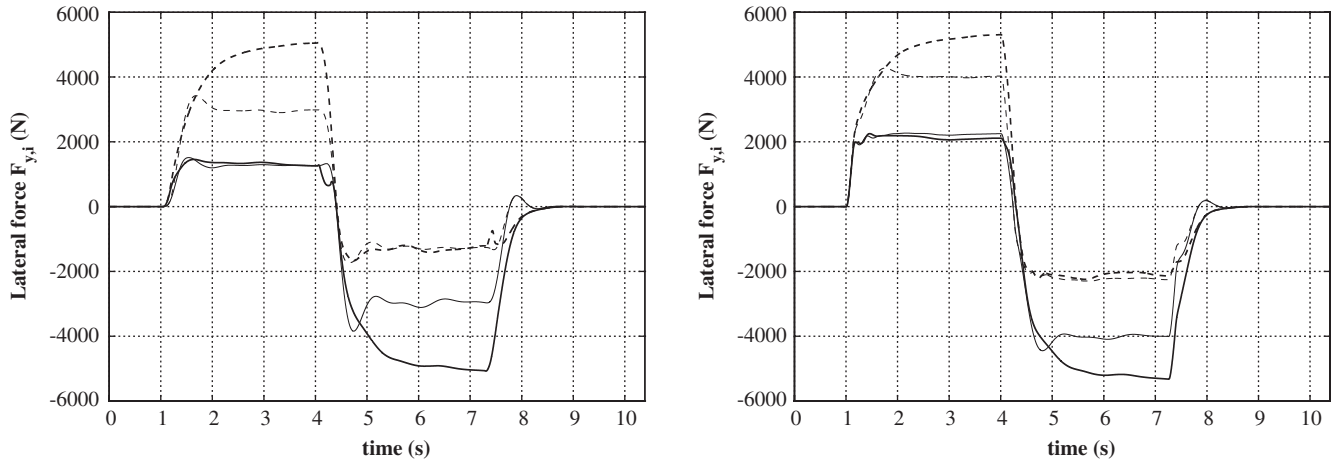


Fig. 24. Light mass vehicle, steer reversal test: vehicle speed: 100 km/h. Handwheel value: 50°. Lateral left (dashed) and right (solid) tyre forces for the controlled and the uncontrolled (thin lines) vehicles. Left picture: rear tyres, right picture: front tyres.

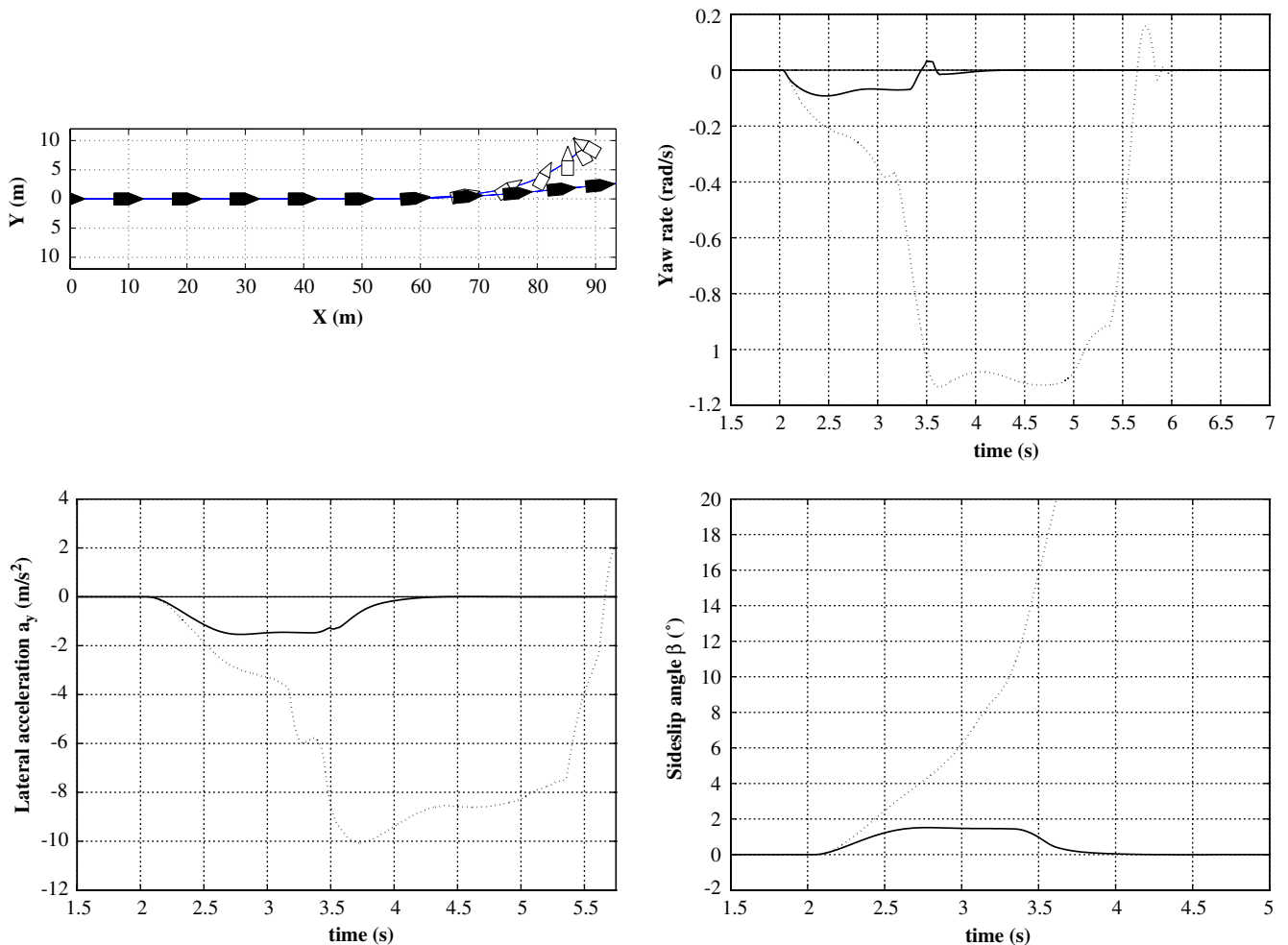


Fig. 25. μ -split braking at 80 km/h, full load controlled (solid) and uncontrolled (dotted) vehicle. Vehicle path (upper left): uncontrolled vehicle (white), controlled vehicle (black).

despite the vehicle mass variation. In particular, the reported yaw rate responses show the significant improvements of the system damping properties for both vehicle

load configurations. Besides, the driving current behaviour shows that the employed control strategy is able to handle effectively actuator saturation as it occurs in all

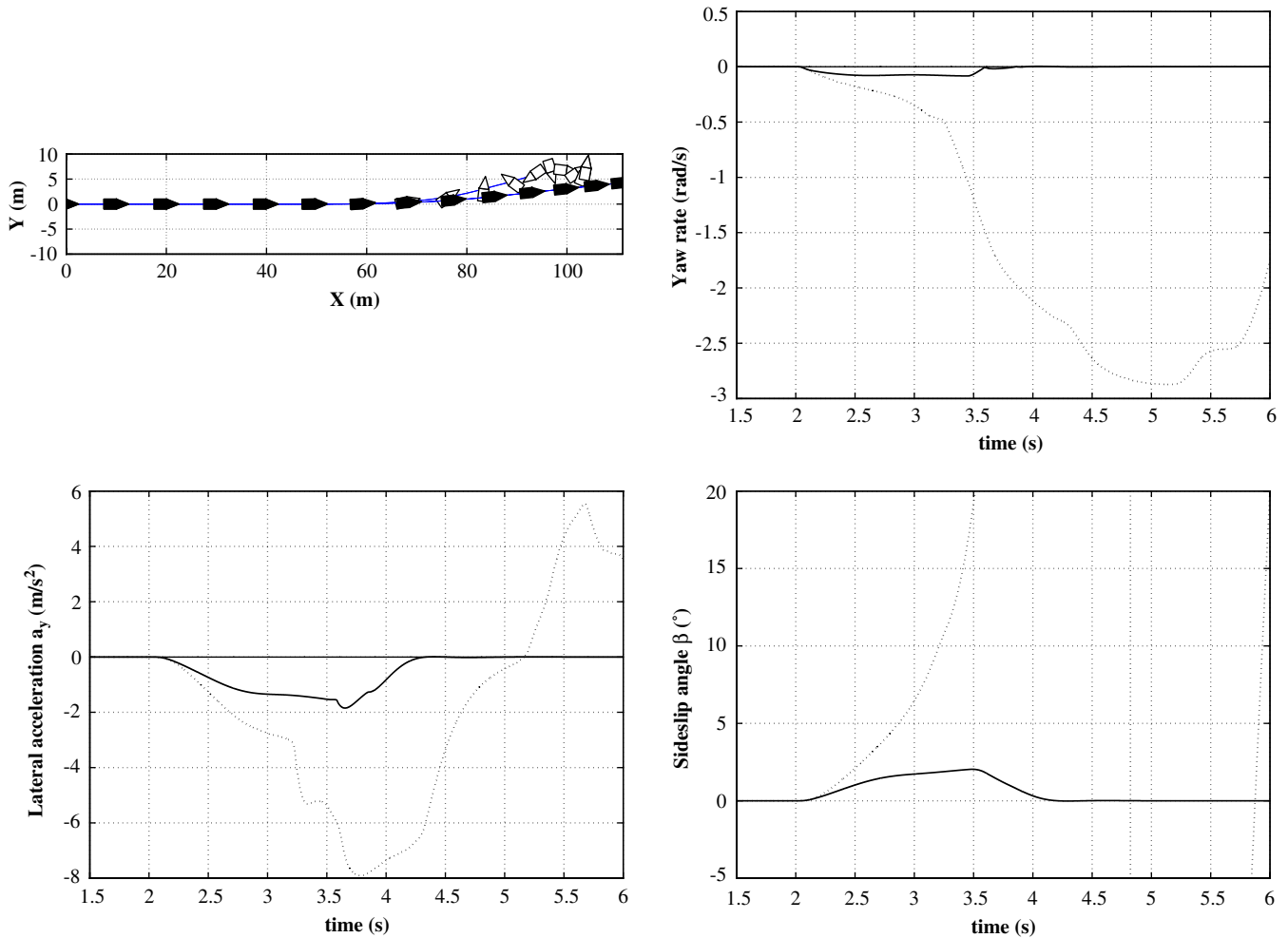


Fig. 26. μ -split braking at 80 km/h, full load controlled (solid) and uncontrolled (dotted) vehicle. Vehicle path (upper left): uncontrolled vehicle (white), controlled vehicle (black).

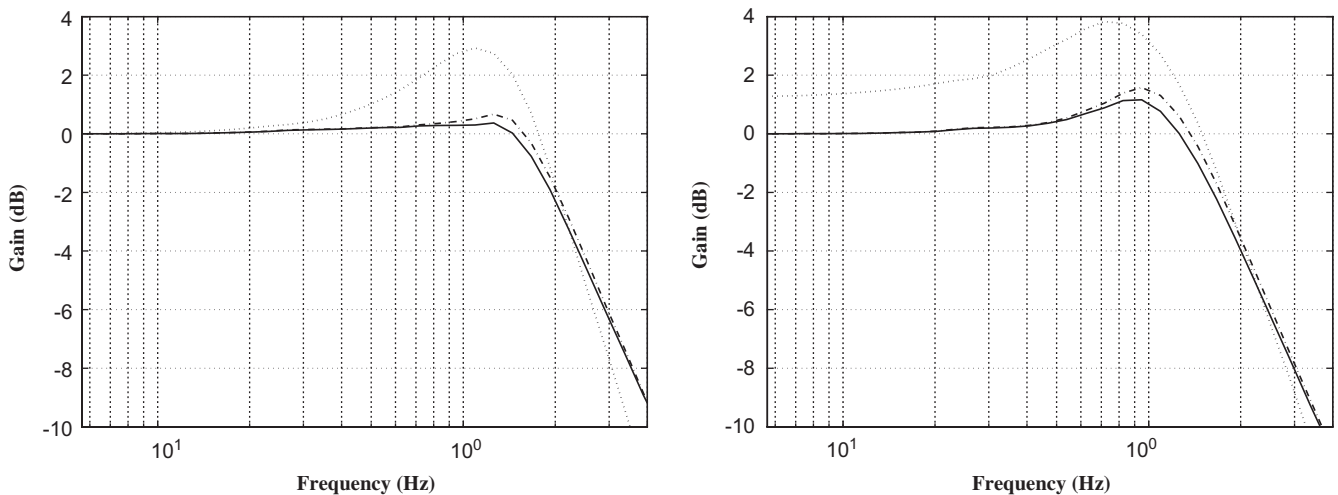


Fig. 27. Steering wheel frequency sweep at 100 km/h: frequency response for the uncontrolled (dotted), basic IMC (dash-dot) and enhanced IMC (solid) vehicle. Left: light mass vehicle, right: full load vehicle.

the performed steer reversal tests (see Figs. 19–22). In particular, the improvements on the vehicle dynamic characteristics achieved by the enhanced IMC structure, with respect to the basic IMC structure of Fig. 11, are quite evident in the full load cases as shown in Figs. 20 and 22, where the more effective input saturation handling properties are put into evidence. Moreover, it can be observed that, according to the understeering curves depicted in Figs. 16 and 17, the controlled vehicle is able to reach higher lateral acceleration and yaw rate values than the uncontrolled one. This means that the controlled vehicle is able to corner with lower radius given the same speed and handwheel input, i.e. its manoeuvrability is increased as shown in Fig. 23 where the vehicle path during a steer reversal test is reported. Sideslip angle β values reached by the controlled vehicle are higher than those of the uncontrolled one: this fact is a consequence of the chosen reference behaviour, which aims to increase the controlled vehicle yaw rate at the expense of higher sideslip angle values. However, as implicitly shown in (15), reference yaw rate can be chosen with different strategies, for example to limit the sideslip angle value reached in the non-linear (i.e. high lateral acceleration) tract, while keeping a lower

understeering gradient in the linear zone. Finally, to make a deeper analysis on the way the RAD device achieves the described performances, a study on the tyre lateral forces has been carried out. In particular, in Fig. 24 the plot of each tyre lateral force $F_{y,i}$ is reported. Both front and rear lateral tyre forces for the controlled vehicle are greater than those of the uncontrolled one, due to the higher lateral acceleration reached, and show better transient damping properties. Moreover, it can be noted that the lateral force increment of the controlled vehicle rear tyres, with respect to the uncontrolled vehicle ones, is greater than that of the front tyres. This difference is the natural consequence of the yaw moment generation demanded by the RAD device: in steady state conditions such yaw moment has the same sign of the vehicle yaw rate (thus reducing the vehicle understeering trend as requested by the designed reference map) and is balanced by a higher increment of the rear tyre lateral forces with respect to the front ones.

In the described μ -split braking manoeuvre the controlled vehicle performances are evaluated in very demanding conditions. The vehicle paths reported in Figs. 25 and 26 show that the proposed control scheme is able to keep vehicle sideslip angle to acceptable low values avoiding

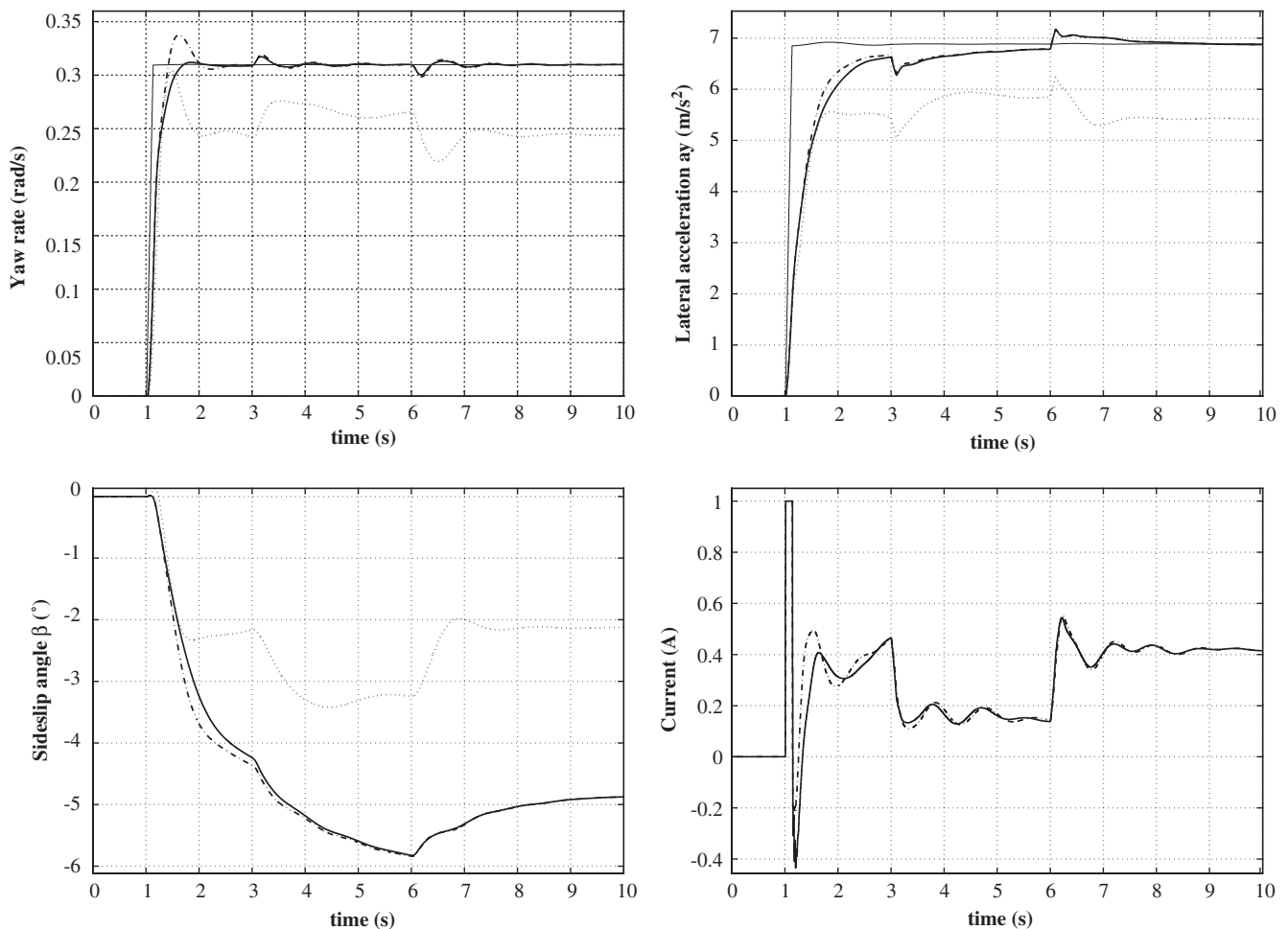


Fig. 28. Step steer test at 80 km/h with 50° handwheel, with increased vehicle mass, wet road and 100 km/h lateral wind disturbance between 3 and 6 s. Comparison between the reference (thin solid line), uncontrolled (dotted), basic IMC (dash-dot) and enhanced IMC (solid) controlled vehicle behaviour.

vehicle instability, while an unstable behaviour occurs in the uncontrolled cases. Note that, despite the emergency features of such manoeuvre, the controlled system besides robustness performances is also able to guarantee quite small values of both a_y and $\dot{\psi}$. The same test performed with the full load vehicle gives results similar to the light mass case (see Fig. 26). Since the basic and enhanced IMC schemes give similar results, only the latter is considered in the reported figures.

In the steering wheel frequency sweep manoeuvre the aim is to evaluate the improvement achieved by the controlled vehicle in terms of resonance peak reduction. In Fig. 27 the simulated behaviour of the transfer ratio:

$$T_m(\omega) = \left| \frac{\dot{\psi}(\omega)}{\dot{\psi}_{\text{ref}}(\omega)} \right|$$

is shown putting into evidence the significant reduction of the resonance peak provided by the proposed control solution with respect to the uncontrolled vehicle, with both load configurations, as well as a slight improvement of the system bandwidth. The basic IMC controller has the same bandwidth of the enhanced IMC scheme but with a higher resonance peak, thus remarking the performance improvement introduced by the proposed control structure.

In Fig. 28 the results of the performed low friction handwheel step manoeuvre, with increased vehicle mass and lateral wind step, show the good disturbance rejection properties of the control system. Note that different tyre-road friction conditions with respect to the nominal one (i.e. dry asphalt) have not been taken into account in the control system design, thus making this manoeuvre a very

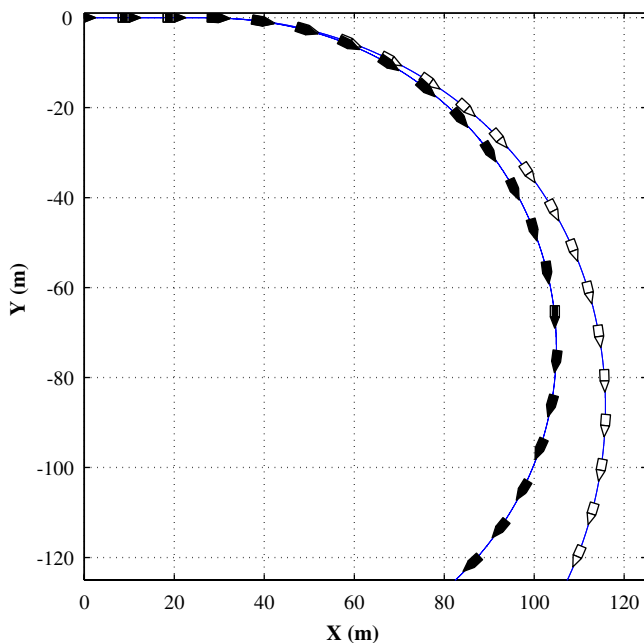


Fig. 29. Uncontrolled (white) and controlled (black) vehicle paths for step steer test at 80 km/h with 50° handwheel, with increased vehicle mass, wet road and 100 km/h lateral wind disturbance between 3 and 6 s.

demanding robustness test. Performances of the enhanced IMC structure are better than those of the basic one also in this context. The uncontrolled and enhanced IMC controlled vehicle paths are reported in Fig. 29.

6. Conclusions

A robust non-parametric approach to vehicle yaw rate control has been presented. The proposed control structure exploits the features of IMC strategies which allow both to guarantee robust stability and to enhance performances in presence of input saturation. A feedforward action has also been included to improve system readiness according to the driver's manoeuvre requests. Simulation results performed on an accurate model of the considered vehicle demonstrate the effectiveness of the proposed control structure. In particular, it has been shown that the achieved performances are very close to the target understeering objectives; a highly damped behaviour in reversal steer and step steer manoeuvres has been obtained; stability is guaranteed in presence of demanding driving conditions like μ -split braking and resonance peak has been significantly reduced in the frequency response. Robust stability properties are also successfully tested in presence of changed and unaccounted road friction conditions.

Acknowledgements

This research was partly supported by the Italian *Ministero dell'Istruzione dell'Università e della Ricerca (MIUR)* under the Research Project of National Interest "Robustness and Optimization techniques for high performances control systems" and by Centro Ricerche FIAT.

References

- Ackermann, J., & Sienel, W. (1993). Robust yaw damping of cars with front and rear wheel steering. *IEEE Transactions on Control Systems Technology*, 1(1), 15–20.
- Ackermann, J., Guldner, J., Steinhausner, R., & Utkin, V. I. (1995). Linear and nonlinear design for robust automatic steering. *IEEE Transactions on Control System Technology*, 3(1), 132–143.
- Assadian, F., & Hancock, M. (2005). A comparison of yaw stability control strategies for the active differential. In *IEEE ISIE*. Dubrovnik, Croatia.
- Avenati, R., Campo, S., & Ippolito, L. (1998). A rear active differential: Theory and practice of a new type of controlled splitting differential and its impact on vehicle behaviour. In *Global powertrain conference*.
- Bakker, E., Lidner, L., & Pacejka, H. B. (1989). A new tyre model with an application in vehicle dynamics studies. In *SAE paper 890087*.
- Börner, M., & Isermann, R. (2006). Model-based detection of critical driving situations with fuzzy logic decision making. *Control Engineering Practice*, 14(5), 527.
- Canale, M. (2004). Robust control from data in presence of input saturation. *International Journal of Robust and Nonlinear Control*, 14(11), 983–998.
- Colombo, D. (2005). Active differential technology for yaw moment control. In *sixth all wheel drive congress*. Austria: Gratz.
- Data, S., & Frigerio, F. (2002). Objective evaluation of handling quality. *Journal of Automobile Engineering*, 216(4), 297–305.

- Frediani, S., Gianoglio, R., & Giuliano, F. (2002). *System for the active control of a motor vehicle differential*. Patent no. US 2002/0016661 A1, Applicant Centro Ricerche Fiat.
- Gaspar, P., Szaszi, I., & Bokor, J. (2005). Reconfigurable control structure to prevent the rollover of heavy vehicles. *Control Engineering Practice*, 13(6), 699.
- Gerhard, J., Laiou, M. -C., Mönningmann, M., Marquardt, W., Lakehal-Ayat, M., & Busch, E. A. R. (2005). Robust yaw control design with active differential and active roll control systems. In *16th IFAC world congress*. Prague, Czech Republic.
- Goodwin, G. C., Graebe, S. E., & Levine, W. S. (1993). Internal model control of linear systems with saturating actuators. In *European control conference*. Groningen, Netherlands.
- Güvenç, B. A., Bünte, T., & Güvenç, L. (2004). Robust two degree-of-freedom vehicle steering controller design. *IEEE Transactions on Control System Technology*, 12(4), 627–636.
- Ippolito, L., Lupo, G., & Lorenzini, A. (1992). *System for controlling torque distribution between the wheels of a common vehicle axle*. EU Patent no. 92121621.4, Applicant Centro Ricerche Fiat.
- Kohen, P., & Ecrick, M. (2004). Active steering—the BMW approach towards modern steering technology. In *SAE Technical Paper No. 2004-01-1105*.
- Malan, S., Milanese, M., Regruto, D., & Taragna, M. (2004). Robust control from data via uncertainty model sets identification. *International Journal of Robust and Nonlinear Control*, 14(11), 945–958.
- Malan, S., Taragna, M., Borodani, P., & Gortan, L. (1994). Robust performance design for a car steering device. In *33rd IEEE conference on decision and control*.
- Milanese, M., & Taragna, M. (2005). H_∞ set membership identification: A survey. *Automatica*, 41(2), 2019–2032.
- Mokhiamar, O., & Abe, M. (2002). Active wheel steering and yaw moment control combination to maximize stability as well as responsiveness during quick lane change for active vehicle handling safety. *Proceedings of the Institution of Mechanical Engineers Part D, Journal of Automobile Engineering*, 216(1), 115–124.
- Morari, M., & Zafiriou, E. (1989). *Robust process control*. Englewood Cliffs, NJ: Prentice-Hall.
- Rajamani, R. (2005). *Vehicle dynamics and control*. Berlin: Springer.
- van Zanten, A. T. (2000). Bosch ESP systems: 5 years of experience. In *SAE Technical Paper No. 2000-01-1633*.
- van Zanten, A. T., Erhart, R., & Pfaff, G. (1995). VDC, the vehicle dynamics control system of bosch. In *SAE Technical Paper No. 95759*.
- Vetturi, D., Gadola, M., Manzo, L., & Faglia, R. (1996). Genetic algorithm for tyre model identification in automotive dynamics studies. In *29th ISATA—International Symposium on Automotive Technology and Automation*. Florence, Italy.
- Vilaplana, M. A., Mason, O., Leith, D. J., & Leithead, W. E. (2005). Control of yaw rate and sideslip in 4-wheel steering cars with actuator constraints. *Lecture Notes in Computer Science*, (vol. 3355, pp. 201–222). Berlin: Springer.
- Zheng, A., Kothare, M. V., & Morari, M. (1994). Anti-windup design for internal model control. *International Journal of Control*, 60(5), 1015–1022.
- Zheng, S., Tang, H., Han, Z., & Zhang, Y. (2006). Controller design for vehicle stability enhancement. *Control Engineering Practice*, 14(12), 1413.